Model for calcite spherulite formation in organic, clay-rich, lacustrine carbonate shales (Barbalha Formation, Aptian, Araripe Basin, NE Brazil)

Marine and Petroleum geology

Model for calcite spherulite formation in organic, clay-rich, lacustrine carbonate shales (Barbalha Formation, Aptian, Araripe Basin, NE Brazil)

Claes H.[1], Miranda T.[2], Falcao T. C.[3], Soete J.[4], Mohammadi Z.[5], Zieger L.[6], Erthal M.M.[3], Aguilar J.[7], Schmatz J.[8], Busch A.[9], Swennen R.[5]

1 Clay and Interface Mineralogy (CIM), RWTH Aachen University, Bunsenstrasse 8, 52072 Aachen, Germany

2 Department of Geology, Federal University of Pernambuco, Recife, PE, 50740-530, Brazil

3 Petrobras Research Center (CENPES), Rio de Janeiro, 21941-915, Brazil

4 Materials Engineering (MTM), Materials Performance and Non-Destructive Testing, KU Leuven, Kasteelpark Arenberg 44, 3001 Leuven, Belgium

5 Earth & Environmental Sciences, KU Leuven, Celestijnenlaan 200E, B-3001 Heverlee

6 Institute of Geology and Geochemistry of Petroleum and Coal (IGGPC), RWTH Aachen University, Lochnerstr. 4-20, 52056 Aachen

7 LAGESED – Departamento de Geologia, Universidade Federal do Rio de Janeiro, Av. Athos da Silveira Ramos, 274, Cidade Universitária, Rio de Janeiro, 21941-915, Brazil

8 MaP - Microstructure and Pores GmbH, Lochnerstrasse 4-20, 52064 Aachen, Germany

9 Lyell Centre, Institute of GeoEnergy Engineering, Heriot-Watt University, Research Avenue South, EH144AS Edinburgh, Scotland, UK

Keywords

Spherulites – Organic matter – Pre-Salt Reservoir Analogue – Microbialites – Barbalha

Abstract

The formation of carbonate spherulites, recognized as part of the South-Atlantic Pre-Salt reservoir rocks, remains enigmatic. Well-chosen analogues provide insights into depositional and diagenetic conditions and the biotic versus abiotic processes that might influence or even control spherulite growth. Radial fibrous calcite spherulites of the Batateira beds in the Barbalha Formation (Aptian, Araripe, NE Brazil) formed mainly in organic and clay-rich laminite layers as nodules that grew around different nuclei, now represented by, amongst others, micrite and apatite ostracods. They vertically alternate with clays, but also carbonate laminites, which locally also contain spherulites. Characterization of the organic matter content of spherulitites (petrography, total organic carbon, vitrinite reflectance, stable isotopes) reveals TOC's of up to 30% related to the presence of mainly oil-prone alginite next to huminite, inertinite, sporinites and zooclasts. The complex mixture of clays, dominantly autogenic mixed layered illite-montmorrilonite, which alternate with lacustrine carbonates and evaporites, is diagnostic for lakes in a semi-arid environment. The occurrence of gypsum, alveolar honeycomb spherulite textures, preferential concentration of pyrite at the spherulite-matrix contact and inward spherulite perforations suggest bacterial activity under shallow and evaporitic syn-depositional conditions. Although the Barbalha spherulites formed chemically-driven in a viscous matrix, the microbial influence, mainly as lamalginite in the clayey matrix, is undeniable. The mixed organic-silicate gel catalyzed calcite spherulite formation. The Barbalha spherulites consequently illustrate the complementary influence of clays, organic matter and evaporitic syn-sedimentary conditions.

1. Introduction

Lacustrine carbonate reservoirs from the Cretaceous South Atlantic basins, including spherulitites, are considered non-conventional and poorly understood, among others, with

regard to biotic versus abiotic precipitation (e.g. Muniz and Bosence, 2015). Despite being one of the most prolific reservoirs discovered in recent times, the number of publications on the characterization of these Pre-Salt reservoir rocks, until 2017, remained strongly limited (Dias, 1998; 2005; Terra et al., 2010; Wright, 2012; Rezende and Pope, 2015; Schröder et al., 2015; Thompson et al., 2015; Saller et al., 2016). A major barrier on the effective studying of the reservoir rocks was the lack of suitable deposits that can be investigated beyond proprietary and confidential drill core material of the South Atlantic (cf. Rogerson et al., 2017). The recent public release of the first core material and associated data, resulted in a strong increase in publication output on the Cretaceous lacustrine South-Atlantic deposits (e.g. Ceraldi and Green, 2017; Herlinger et al., 2017; Althaus et al., 2019; Bertolini et al., 2019; Farias et al., 2019; Lima et al., 2019; Amarante et al., 2020; Pietzsch et al., 2020; Pocas Belila et al., 2020; Wright and Barnett, 2020).

Due to the ultra-deep scenario of exploration and the associated lack of continuous pre-salt outcrops, reservoir information on lateral and vertical variation between seismic and core-scale remains a problem and highlights the importance of reservoir analogues. While it is difficult, if not impossible, to find analogues that cover the entire depositional and diagenetic complexity of the Pre-Salt deposits, worldwide fieldwork, experimental and modelling studies are able to provide insights addressing specific points of view, i.e. on the microbial or abiotic depositional processes (e.g. Bahniuk et al., 2015; Catto et al., 2016; Bouton et al., 2016; Chafetz et al., 2018; Kirkham and Tucker, 2018), the sedimentology (e.g. Seard et al., 2013; Awramik and Buchheim, 2015; Ronchi and Francesco, 2015; Rogerson et al., 2017; Mercedes et al., 2017; Valente et al., 2017), diagenesis (e.g. Gindre-Chanu et al., 2016; Claes et al., 2017a; De Boever et al., 2017), geochemistry (e.g. Teboul et al., 2016; 2017; 2018; Tutolo and Tosca, 2018; Claes et al., 2019), petrophysical characteristics (e.g. Muniz and Bosence, 2015; Soete et al., 2015, 2017; Claes et al., 2017b; Regnet et al., 2018; Hosa et al., 2019) or structural

aspects (Van Noten et al., 2013, 2019; Miranda et al., 2018; Török et al., 2019). Only the assembly and integration of information from different analogue sites with the core, sidewall core, borehole, well and seismic reservoir data leads to a proper understanding of the Pre-Salt reservoirs to support their exploitation (Virgone et al., 2013). The success of the assembly strategy for understanding the Pre-Salt and its economic value depends on selecting and studying suitable analogues.

The Aptian lacustrine deposits in the Barbalha formation of the Araripe Basin are almost time-equivalent to the Pre-Salt reservoirs and contain spherulitites, the major focus of this study. To avoid confusion, distinction in terminology is made between the individual (sub)spherical allochems with smooth or lobated rims, i.e. the spherulites, and the rock containing spherulites, i.e. a spherulitite (Terra et al., 2009). The Araripe spherulites are best developed in the Batateira Beds and are described as "*peloids in paperthin shales*" (Chagas et al., 2007) and "*millimetric to centimetric microbial carbonate laminae and nodules*" (e.g. Scherer et al., 2015; Fambrini et al., 2019). The Batateira beds, named by Hashimoto et al. (1987), are defined as plumbiferous (Farin, 1974), black bituminous shales with carbonate sheets of algal origin, coprolites, ostracods and fish remains (Assine, 1992 and 2007; Assine et al., 2014) and reflect deposition in an anoxic, low energy lacustrine system (Scherer et al., 2015; Fambrini et al., 2019) in a semi-arid region (Lima and Perinotto, 1984). The Batateira beds occur as an important stratigraphic marker of 10m thick black shale-carbonate mixed interval continuous over at least 20km in the Araripe Basin (Chagas et al., 2007; Fabrini et al., 2019), but are possibly even continuous into neighboring basins (see discussion including Varejao et al., 2016). Spigolon et al. (2015) evaluated the petroleum composition and confirmed the source rock potential of the Batateira spherulitites.

This study aims to provide a sedimentological characterization of the Barabalha lacustrine spherulitites in order to understand their depositional and early diagenetic syngenetic

conditions and formation mechanisms. The basis is a multi-disciplinary approach, including fieldmapping and logging, petrography, TOC, vitrinite reflectance and carbonate and organic matter stable isotope analyses. The authors, besides outcrops of the Barbalha Formation, visited lacustrine outcrops of the covering formations, mainly the Crato Formation, in order to be able to consider the observations in a larger frame. Given the ongoing discussions on the microbially mediated versus the dominantly abiotic silica gel nucleated origin of the Barra Velha and Macabu Pre-Salt spherulites (e.g. Dorobek et al., 2012; Wright and Barnett, 2015; Kirkham and Tucker, 2018; Wright and Barnett, 2020) and the discussion of an open deep lake versus closed shallow lake scenario (Mercedes-Martin et al. 2019 and Wright and Barnett 2020, respectively), the Barbalha Formation might form a geographically proximal and possibly genetic analogue, and/or can provide additional information on the settings in which spherulites can form. This is not only of use for the Pre-Salt hydrocarbon reservoirs but also for other worldwide spherulite deposits, like, for example, in the Precambrian of Arctic Norway (Meinhold et al., 2019).

2. Geological setting

The study area is located at the northern border of the Araripe Basin (Fig. 1), which is the largest intraplate basin of Northeast Brazil (Castro and Castelo Branco, 1999). The tectonic evolution of this basin is related to the break-up of Gondwana and subsequent South Atlantic rifting (Matos, 1999). The underlying basement rocks are dominantly Archean orthogneisses (Granjeiro Complex), ranging in composition from quartz diorite to granite, but meta-ultramafics, meta-gabbros, amphibolites and Neoproterozoic meta-sedimentary rocks (Cachoeirinha Group) locally occur, as well as a Cambrian granitic intrusion (Celestino et al., 2020). The basin has an E-W-elongated shape and is bounded to the north by the Triunfo Fault, which represents the brittle reactivation of the Patos shear zone (Celestino et al., 2020).

126 The stratigraphy of the Araripe Basin can be divided into five tectono-sedimentary
127 sequences, namely: a) Paleozoic, represented by the Ordovician-Devonian continental deposits
128 of the Cariri Formation; b) prerift, represented by the Tithonian continental deposits of the
129 Brejo Santo and Missão Velha Formations; c) rift, composed of the Neocomian continental
130 deposits of the Abaiara Formation; d) postrift I, known as the Santana Group which includes
131 the Aptian (Arai and Assine, 2020) continental deposits of the Barbalha (before referred to as
132 the Rio da Batateira; Ponte and Appi, 1990), Crato, and Ipubi formations and the lacustrine to
133 marine deposits of the Romualdo Formation; and e) postrift II, which includes the Albian-
134 Cenomanian continental deposits of the Araripina and Exu formations (Assine, 2007; Assine
135 et al., 2014) (Fig.1).
136 This study focusses on the lacustrine spherulites of the early Aptian in the Barbalha
137 Formation (P-270 biozone; Lima and Perinotto, 1984). The Barbalha Formation consists of
138 two main sequences of fluviatile sandstones to mudstones that grade into lacustrine black
139 shales. The first sequence culminating in the black-shale-carbonate mixed interval of the
140 Batateira beds, is unconformably interrupted by a renewed fluvial system (Hashimoto et al.,
141 1987; Assine, 1992; Chagas et al., 2007; Assine, 2007; Scherer et al., 2015; Fambrini et al.,
142 2019). The upper sequence of the Barbalha Formation grades transitionally into the Crato
143 Formation (Fambrini et al., 2019) which represents the main lacustrine phase of the continental
144 succession of the Araripe Basin (Neumann et al., 2003). Fieldwork included a new outcrop of
145 the Barbalha Formation in the northern part of the Araripe Basin (Fig. 1), in addition to the
146 stratigraphic logs previously studied by a.o. Scherer et al. (2015) and Fambrini et al. (2019).
147 Sampling for further analyses focused on the Batateira beds of the Barbalha Formation from
148 the outcrop indicated in Figure 1.
149

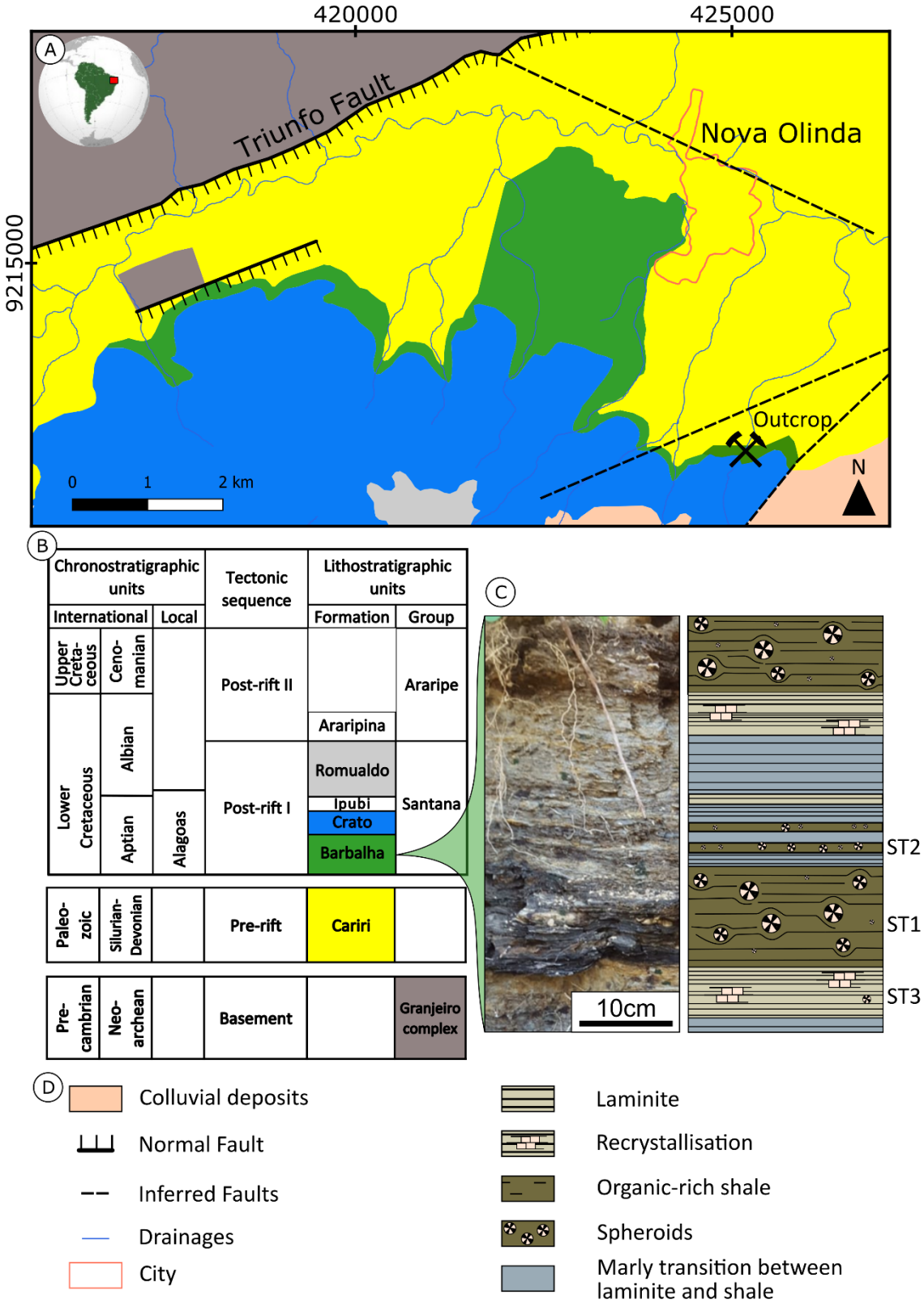

Figure 1: A) Geological map of the area around the sampled outcrop in the north of the Araripe Basin. B) Stratigraphy of the encountered lithologies in A. C) Representative

outcrop section of the Batateira Beds in the middle of the Barbalha Formation with sample types indicated; ST1:Organic-rich carbonate shale spherulitites with micritic nuclei (Fig. 2). ST2:Organic-rich carbonate shale ostracod-rich spherulitites (Fig. 3). ST3: Carbonate laminite with spherulites (Fig. 5). Legends of A and C.

3. Methods

3.1 Petrography

Because of the fragility of some of the samples, all were doubly impregnated under vacuum with resin before thin-section (KU Leuven) and polished section (RWTH Aachen) preparation. A fluorescent dye was used in order to easily distinguish (micro-)porosity with incident fluorescent light microscopy. Polishing was done with oil to avoid clay swelling. Thin-sections were scanned with parallel and crossed polarized transmitted light and incident light at a resolution of 600 dpi on an EPSON scanner with an EPSON film adapter (Seiko Epson Corporation, Nagano, Japan) at the KU Leuven. Petrographic characterization (KU Leuven) was conducted on an Olympus BX60 (Olympus Corporation, Tokyo, Japan) and Leica DM LP Parallel (Leica Microsystems, Wetzlar, Germany) and Crossed Polarizer Optical and Fluorescence light (PPL, CPL and FL respectively) microscope. Cold cathodoluminescence (CCL) observations were carried out using a Zeiss MK5-2 microscope under 10 KeV and 250 mA. Reflectance measurements (RWTH Aachen) were performed using a Zeiss Axioplan incident light microscope at λ =546 nm equipped with a 50×/0.85 Epiplan-NEOFLUAR oil immersion objective. Random huminite reflectance (HR_r) measurements were conducted according to the standard procedure described in Taylor et al. (1998). Each measurement was calibrated with a Leuco Saphire standard (VR_r=0.592%). Samples for SEM (RWTH Aachen) were Ar-ion polished using a Leica EM TIC3X Broad Ion Beam (BIB) polisher with a rotary stage at low angle with respect to the sample surface and 6 kV acceleration voltage for 1h,

179 followed by a tungsten coating of ~7.5nm to make the specimen conductive for high-resolution
180 imaging. Zeiss Supra 55 FE and FEI Versa 3D Dual Beam field emission scanning electron
181 microscopes (SEM) were used for imaging. Both microscopes were equipped with secondary
182 electron (SE), backscattered electron (BSE) and energy dispersive X-ray (EDX) detectors,
183 allowing for the simultaneous collection of image data and element concentrations to identify
184 different minerals.
185
186 *3.2 QEMSCAN*
187 QEMSCAN (Quantitative Evaluation of Materials by SCANning electron microscopy),
188 (FEI/Thermo corporate headquarters, North America Nanoport, Hillsboro, OR, USA) analysis
189 was applied with a beam voltage of 15.0 keV and a Bruker XFlash 5030 detector (RWTH
190 Aachen). The horizontal and vertical point spacing (height and width of a pixel) is 4.76 µm.
191 The requested field size is 1500 µm (width and height each). The total field size is 29 mm
192 height and 20 mm width. 2000 X-Ray counts were detected per pixel.
193
194 *3.3 X-Ray Diffraction (XRD)*
195 The full XRD analyses were performed at RWTH Aachen. Rock samples were crushed
196 manually in a mortar and subsequently milled with a McCrone Micronising mill for 20 minutes
197 to ensure uniform crystallite sizes. Milling was done in ethanol to avoid dissolution of water-
198 soluble components and strain damage to the samples. An internal standard (Corundum, 20 wt.
199 %) was added to improve the accuracy of the analysis. Bulk mineralogical compositions were
200 derived from X-ray diffraction patterns measured on randomly oriented powders. For textured
201 clay samples, the clay fraction was separated with the Atterberg method after removal of
202 carbonates, organic matter and iron oxides (procedures from Moore and Reynolds, 1997 and
203 Lagaly et al., 1997). ~100 mg clay sample was dispersed in 3 mL H_2O. Two suspensions are

made from the Mg-exchanged clay fraction. To one of them two to three drops of glycerol or a drop of glycerin were added. Both suspensions were ultrasonically treated for >10 minutes in order to obtain a stable suspension. The suspensions are spread onto porous ceramic, glass or silica mono-crystal plates. For both bulk and oriented samples, the measurements were done on a Bruker AXS D8 Advance diffractometer using CuKα-radiation produced at 40 kV and 40 mA and a Huber Guinier diffractometer using CoKα-radiation at 40 kV and 30 mA. The divergence slit is fixed at 1 mm, with a secondary Soller slit behind the sample. The detector is a scintillation counter with graphite monochromator. Diffractograms of bulk samples were recorded from 2° to 92° 2θ in 0.02° steps and a counting time of 5 s. Textured samples are complemented by measurements of glycerol added and 500 °C heated samples with diffractograms recorded from 2° to 40° 2θ in 0.02° steps and a counting time of 5 s.

Quantitative phase analysis was performed by Rietveld refinement using Profex 4.0.0 BGMN software, with customized clay mineral structure models (Ufer et al., 2008).

3.4 Total Organic Carbon (TOC)

15 mg of each sample were weighed into 9 × 5 mm Ag cups, and carbonates were removed by repeated acidification with diluted (2%) HCl. For the determination of %OC (organic carbon), %N (nitrogen) and the stable carbon isotope composition of the OC fraction ($\delta^{13}C_{OC}$), samples were combusted in an elemental analyser–isotope ratio mass spectrometer (EA-IRMS, ThermoFinnigan Flash HT, and ThermoFinnigan DeltaV Advantage), and data were calibrated using an in-house Leucine and IAEA-C600 standard (caffeine) at the KU Leuven. Two samples were selected for exploratory Rock-Eval analysis (RWTH Aachen), using a Girdel Rock-Eval MK II pyroanalyzer.

3.5 Stable isotopes

Samples for stable oxygen and carbon isotopes were analysed at the KU Leuven on a Thermo Delta V Advantage isotope ratio mass spectrometer coupled to a GasBench II. Spherulites were handpicked from their matrix before being crushed. Samples were flushed with helium and reacted with 100% phosphoric acid to produce CO_2 gas and were allowed to react for 24 h at 25 °C to reach isotopic equilibrium. Data from each run were corrected using the regression method with LSVEC ($\delta^{18}O$ = −26.7‰, $\delta^{13}C$ = −46.6‰), NBS-19 ($\delta^{18}O$ = −5.01‰, $\delta^{13}C$ = −23.2‰), and NBS-19 ($\delta^{18}O$ = −2.2‰, $\delta^{13}C$ = +1.95‰) as standards, as well as using two in-house $CaCO_3$ standards, which were regularly calibrated against NBS-19 and LSVEC. Long-term standard deviations were better than 0.1‰. Both $\delta^{18}O$ and $\delta^{13}C$ values of samples are expressed relative to Vienna-Pee Dee Belemnite (V-PDB).

3.6 Computer Tomography (XCT)

XCT image acquisition was performed at the KU Leuven on a Phoenix Nanotom S (GE Measurement and Control Solutions, Wunstorf, Germany), equipped with a 180 kV/15 W nanofocus X-ray tube and a 2304 x 2304 pixels Hamamatsu detector, with a 5 µm pixel pitch. An acceleration voltage of 70 kV and a current of 500 µA, in nanofocus mode 0, were applied to generate the X-rays using a tungsten target. A 0.1 mm thick copper filter was installed during the scans. Radiographic projections were acquired for a 360° rotation sector, with a 0.2° rotation step. The exposure timing was set to 500 ms. The acquisition time was only 15 minutes in fast-scan mode, which allows for a continuous sample rotation. The filtered-back projection algorithm in the Phoenix datos|x 2 reconstruction software (GE Measurement and Control Solutions, Wunstorf, Germany) was used to reconstruct all the sectional planes of the generated image stack, until finally a 3D model of the sample was generated. The resulting 3D model has an isotropic voxel size of 9 µm. The XCT images were segmented, visualized and analysed in Avizo 2019.1 (Thermo Fisher Scientific, Hillsboro, Oregon, USA).

4. Results

4.1 Spherulites in organic-rich carbonate shales

The Araripe spherulites (mm up to cm scale) most commonly occur in the clayey (clay content reaches up to 50%), exceptionally organic rich (TOC up to 30%), anastomosingly laminated shaly carbonate matrices (Figs. 2 and 3) of the Batateira beds. The spherulites consist of radial fibrous calcite crystals with intercrystalline microporosity (e.g. Fig. 3H-K). Their nuclei can be composed of anhedral micrite (Fig. 2) but are also related to other substrates, like apatite-calcite ostracods in ostracod-rich lithologies (Fig. 3). Both valves of the ostracods occur together. Under crossed polar configuration, the spherulites show the typical cross extinction (Fig. 2D & F and 3B, D & G). The spherulites and ostracods are bright yellow to light brown under Cold Cathodoluminescence as opposed to their dark matrix (Fig. 2G, 3E & H). The spherulite size, even within a hand sample is highly variable (Fig. 2 and 3, in particular 2N) and observations from classical petrography and SEM show growth competition, as illustrated in Figure 2H. The matrix laminae bend and wrap around the spherulites. µCT revealed perforations from the edge towards the inside of the spherulites (Fig. 2K). At the contact between the spherulites and the matrix, siderite, iron oxides (goethite) and sometimes pyrite (Fig. 2L) are concentrated. Pyrites are also observed to less extent inside the matrix of the spherulitites. The clay fraction of the spherulitite samples is a complex mixture of dominantly illite, smectite (mainly montmorrilonite), chlorite and kaolinite (Fig. 4, Table 2). The main phase has been determined as interstratified illite – montmorillonite (Fig. 4). Gypsum and minor amounts of siderite occur in association with the laminated shale matrix together with clay to silt-sized detrital quartz and feldspar. Furthermore, these spherulite-rich beds are associated with larger centimeter to decimeter scale carbonate concretions. The matrix-based organic matter mainly consist of amorphous organic matter (AOM) from algae (alginite),

279 which corresponds to highly oil-prone type I kerogen (Hydrogen Index > 500 mg HC/ g TOC,
280 T_{max} > 400°C). Within the fabrics of the spherulites, alveolar honeycomb features are observed
281 (Fig. 2J).

282 The Barbalha shaly matrix surrounding the spherulites display $\delta^{18}O$ signatures that vary
283 from -8 to -7‰ and from -3 to -5‰ for $\delta^{13}C$ and $\delta^{13}C_{org}$ of -24 to -29‰ (Table 1). The
284 relatively low amount of associated nitrogen (0.5-0.8%) results in high C/N ratios of 33 to >36.
285 Successful $\delta^{15}N_{org}$ measurements varied between 0 and 4‰ (Table 1).

286 The spherulites show similar $\delta^{18}O$ signatures to their matrix (-8 to -6‰). In most cases
287 the $\delta^{13}C$ signatures are slightly lower (-4 to -5‰), with exception of a few spherulites in an
288 ostracod matrix (<-6‰; ~2‰ difference; Table 1). The $\delta^{13}C_{org}$ varies between -25 and -22‰.
289 The nitrogen reaches maximally 0.13%, resulting in C/N ratios from 6 to >37. $\delta^{15}N_{org}$ varies
290 between 0 and 2.8‰ (Table 1).
291
292 *4.2 Spherulites in carbonate laminites*
293 The Barbalha laminites are low porous carbonate mudstones that show a macro-scale
294 lamination of beige and greyish-brownish carbonate laminae (0.3-3mm thick) and locally
295 contain crustiform to spherical concretions (Fig. 5). Massive horizontally elongated
296 concretions with concentric growth laminae can be distinguished from agglomerative and
297 individual radial fibrous spherulites. Laminae anastomose around the concretions and
298 spherulites. On micro-scale the matrix consists of peloidal micrite ghost grains that
299 recrystallized into microspar. The laminites occur as laterally continuous, few to tens of
300 centimeter thick, intervals intercalated with the shaly spherulitites. With a TOC of ~2%, the
301 organic matter content of the laminites is considerably lower compared to the shaly
302 spherulitites. The laminites and the spherulites inside consist of almost purely (>90%) calcite
303 (Table 2). Darker laminae are associated with iron and/or manganese oxides (Fig. 5). The latter

304 also occur preferentially at the spherulite-matrix interface and, more inward the spherulite
305 concretions, some pyrite is observed. Apatite occurs related to local organic matter lenses and
306 fossil fragments. Minor amounts of clay, quartz and feldspar grains are identified from XRD
307 and QEMSCAN.

308 The spherulite $\delta^{18}O$-$\delta^{13}C$ values (-7.8‰ for both) differ from those of their laminite
309 matrix ($\delta^{18}O$ of -7‰ and -2‰ for $\delta^{13}C$). The laminite matrices, with 0.08-0.09% nitrogen,
310 have a C/N ratio of 19.7 to 23.1 and $\delta^{13}C_{org}$ -25‰ and $\delta^{15}N_{org}$ of 4.5 to 5 (Table 1).

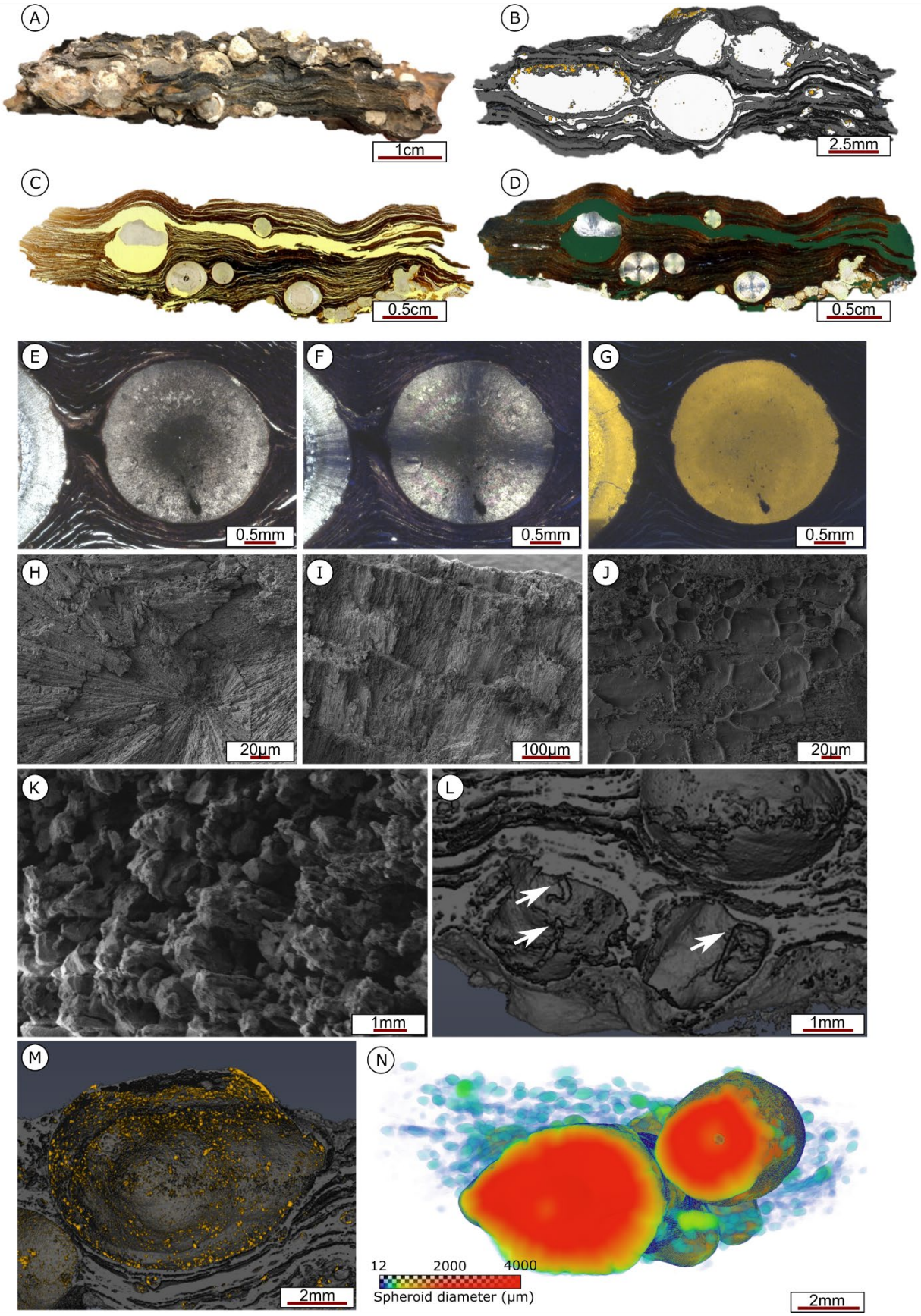
A
1cm
B
2.5mm
C
0.5cm
D
0.5cm
E
0.5mm
F
0.5mm
G
0.5mm
H
20µm
I
100µm
J
20µm
K
1mm
L
1mm
M
2mm
N
12
2000
4000
Spheroid diameter (µm)
2mm

311

Figure 2: Images of spherulites with micritic cores in an organic-rich (up to 30%), clay-rich laminites. A) Outcrop spherulitite sample with wavy lamination of the dark matrix surrounding white spherulites. B) Rendered µCT image with segmentation of the different phases, i.e. calcite in white, matrix in black and iron oxides and/or pyrite in yellow. C) and D) Thin-section scans of spherulitite sample with micritic cores under PPL and CPL, respectively. Notice the typical cross extinction of the spherulites under CPL. E), F) and G) Micro-petrographic images of spherulites in the organic-rich, clay-rich matrix under PPL, CPL and CCL, respectively. Notice how the laminae of the matrix bend around and wrap the spherulites. H) SEM image illustrating the competitive growth of radial fibrous spherulites. I) SEM image showing the different growth layers of fibrous crystals forming the spherulite. J) SEM image showing hexagonal / alveolar honeycomb texture within the spherulite. K) SEM image illustrating the intercrystalline microporosity related to the spherulites. L) Rendered µCT image of the segmented matrix. Removal of the segmented spherulites reveals perforations from the edge inwards the spherulites. M) Rendered µCT image of the segmented matrix and iron oxides and/or pyrite. Removal of the segmented spherulites emphasizes the preferential occurrence of the iron oxides/sulfides on the contact between the spherulites and their matrix. N) Rendered µCT image of zone within a spherulitite sample with spherulites colored according to size.

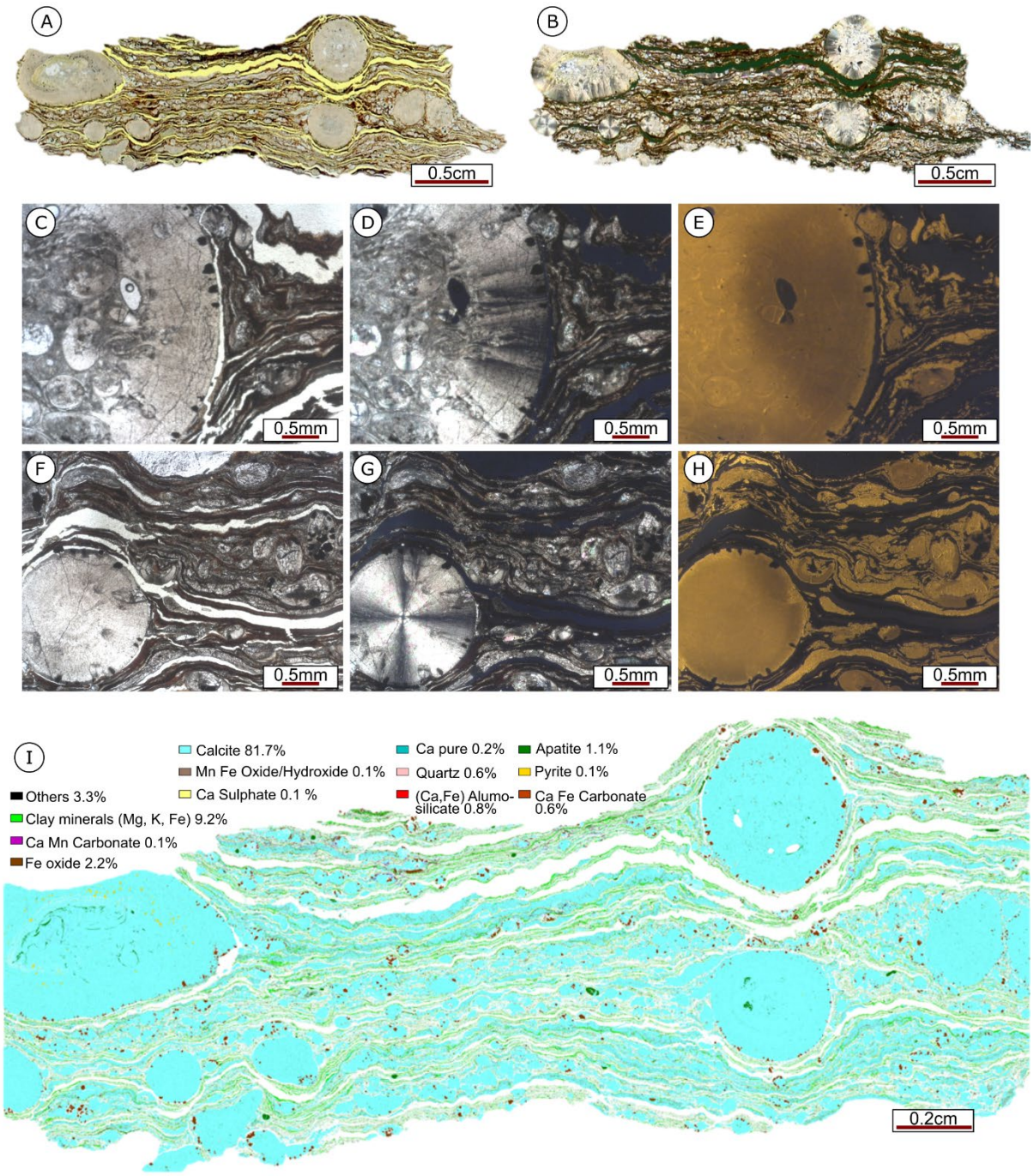

330

331 F*igure 3: Spherulites with ostracod nucleus. A) and B) Thin-section scans of*

332 *spherulitite sample rich in ostracods under PPL and CPL, respectively. C), D) and E) Micro-*

333 *petrographic images of spherulite edge with ostracods in its nucleus and surrounding matrix*

334 *in PPL, CPL and CCL, respectively. Notice how the laminae bend around the spherulite. F),*

335 *G) and H) Micro-petrographic images of spherulite in an ostracod rich matrix in PPL, CPL*

336 *and CCL, respectively. I) Results of QEMSCAN analysis of the thin-section shown in A and B*

337 *with mass percentages of minerals given. Note that despite the use of oil for thin-section*

338 *preparation, part of the matrix (mainly clays and organic matter) was lost.*

339

340

341 *Table 1: Results geochemical analyses (ND = not determined).*

Sample	Lithotype / Description	%C	%N	C/N	$\delta^{13}C_{Org}$‰	$\delta^{15}N_{Org}$‰	$\delta^{13}C$‰	$\delta^{18}O$‰
Araripe1	Shaly spherulitite matrix	27.17	0.79	34.57	-24.7	4.0	-3.33	-7.96
Araripe2	Shaly spherulitite matrix	28.99	0.80	36.08	-24.3	3.7	ND	ND
Araripe3	Spherulite in shaly matrix	0.37	0.06	6.67	-24.1	2.4	-4.05	-7.67
Araripe4	Spherulitev in shaly matrix	5.01	0.13	37.48	-22.1	ND	-4.74	-7.61
Araripe5	Spherulite in shaly matrix	ND	ND	ND	ND	ND	-3.67	-6.99
Araripe6	Spherulite in shaly matrix	ND	ND	ND	ND	ND	-4.63	-8.22
Araripe7	Spherulite in shaly matrix	ND	ND	ND	ND	ND	-4.91	-7.63
Araripe8	Shaly spherulitite matrix with ostracods	22.28	0.66	33.61	-28.8	ND	-4.97	-6.95
Araripe9	Shaly spherulitite matrix with ostracods	22.93	0.67	34.46	-28.5	0.0	-5.09	-6.87
Araripe10	Shaly spherulitite matrix with ostracods	16.74	0.50	33.72	-28.7	0.0	-5.12	-6.62
Araripe11	Shaly spherulitite matrix with ostracods	18.38	0.53	34.84	-28.7	ND	-5.19	-6.82
Araripe12	Spherulite in ostracod-rich matrix	1.20	0.08	15.16	-24.8	0.4	-5.93	-6.69
Araripe13	Spherulite in ostracod-rich matrix	0.56	0.05	11.35	-24.1	2.8	-6.42	-7.03
Araripe14	Spherulite in ostracod-rich matrix	0.72	0.09	8.29	-24.3	ND	-6.29	-7.02

Araripe15	Spherulite in ostracod-rich matrix	0.37	0.06	6.04	-24.6	2.5	-4.28	-6.99
Araripe16	Spherulite in ostracod-rich matrix	ND	ND	ND	ND	ND	-5.51	-5.71
Araripe17	Spherulite in ostracod-rich matrix	ND	ND	ND	ND	ND	-4.81	-6.92
Araripe18	Laminite – spherulitite matrix	1.77	0.09	19.74	-25.0	4.5	-2.22	-7.06
Araripe19	Laminite – spherulitite matrix	1.95	0.08	23.10	-25.0	5.0	-2.08	-7.04
Araripe20	Grey-Blueish spherulite in laminite – spherulitite	ND	ND	ND	ND	ND	-7.77	-7.83

342

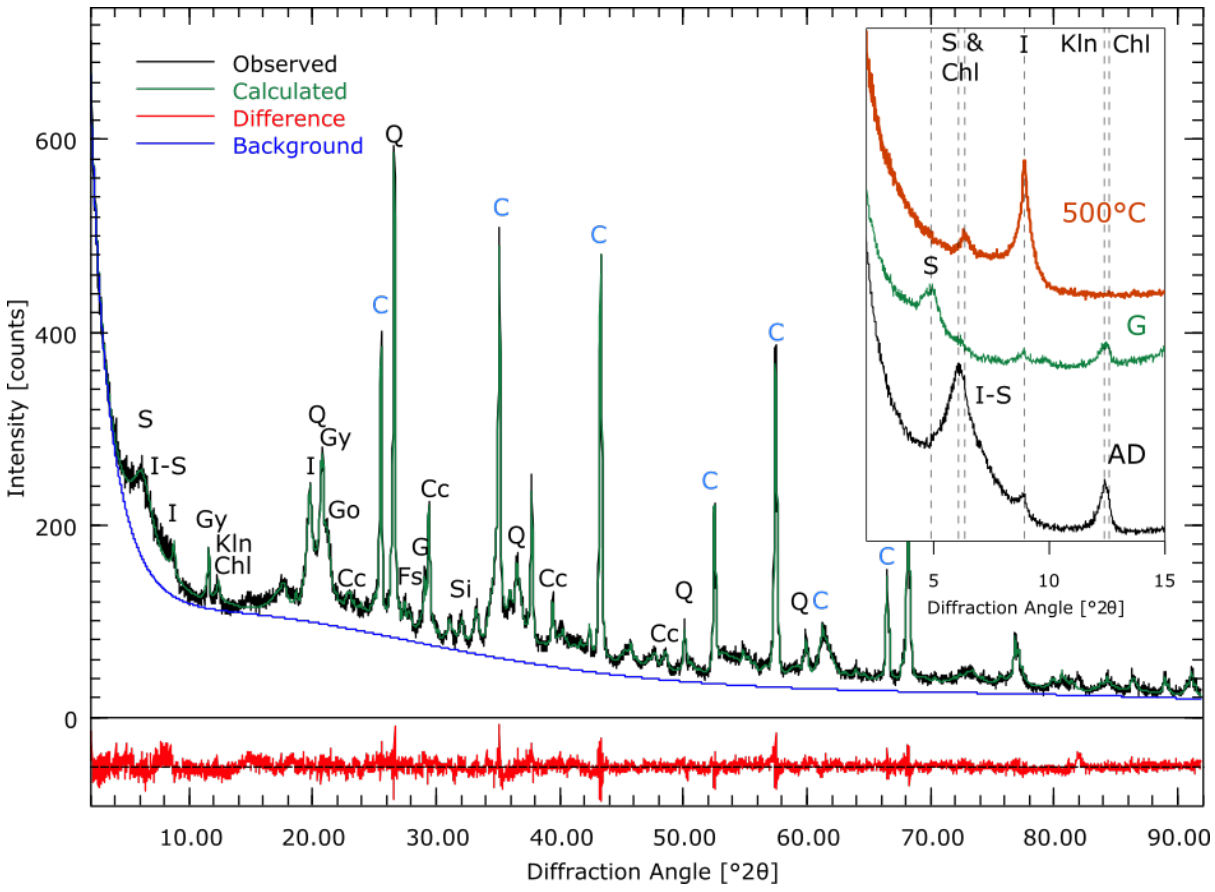

343

Figure 4: Representative XRD diffraction pattern for the shaly matrix of spherulites with micritic nucleus with inset of textured clay fraction diffraction patterns of Air Dried (AD), Glycerin added (G) and 500°C heated (500°C) samples. Together with the (060) reflection at 1.5A, the smectite was determined as mainly montmorillonite. Notice the high background due to the presence of organic matter in the sample. Quantification was further verified after removal of carbonates, organic matter and iron oxides. The main peaks of the minerals are highlighted for internal standard Corundum (C), Calcite (Cc), Chlorite (Chl), Feldspar (Fs), Goethite (Go), Gypsum (Gy), Illite (I), interstratified Illite-Smectite (I-S), Kaolinite (Kln), Quartz (Q), Smectite (S), Siderite (Si).

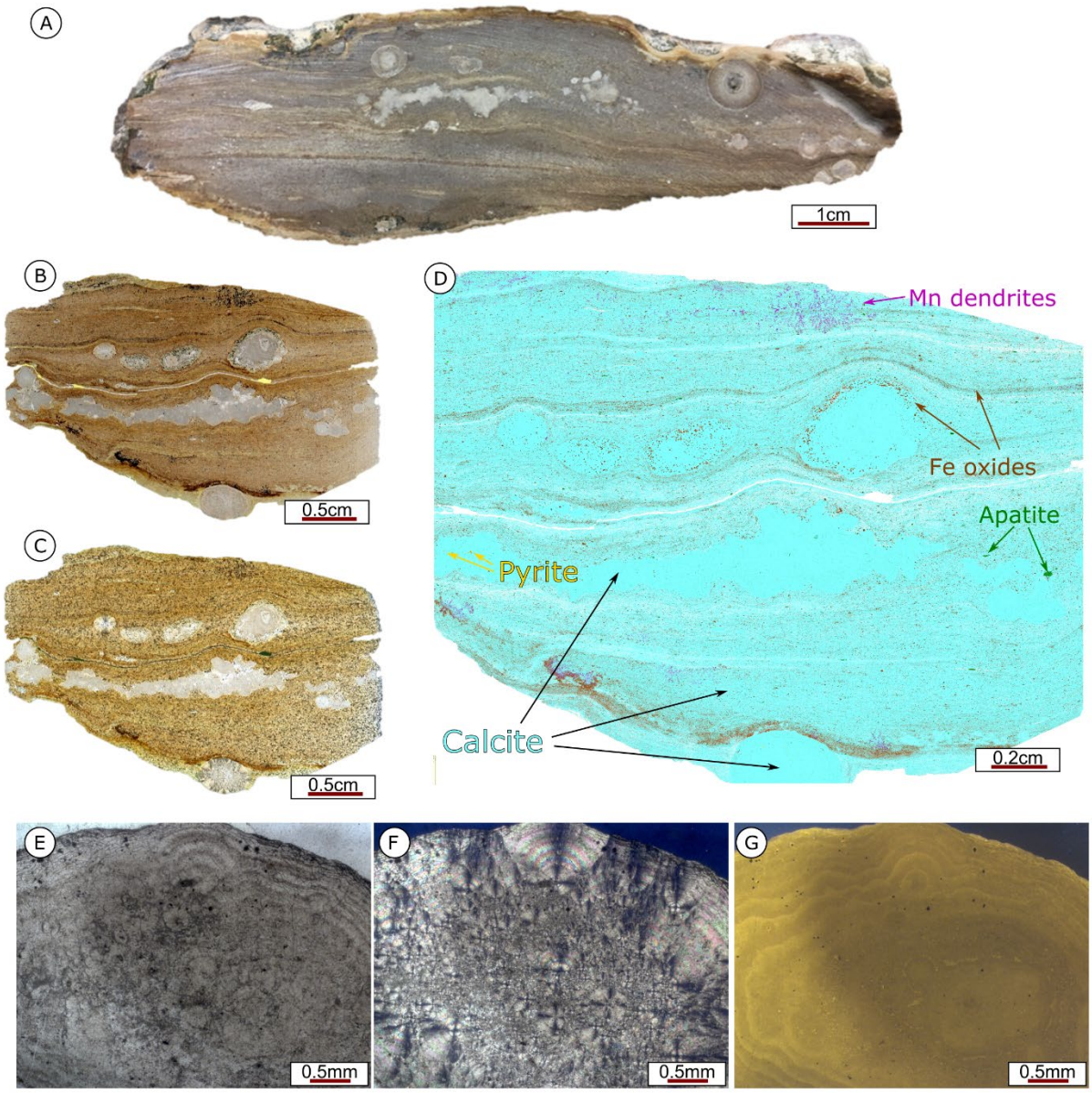

353

354 *Figure 5: Spherulites in carbonate laminites. A) Hand specimen of laminite with*
355 *carbonate concretions and spherulites. B) and C) Thin-section scans of laminite sample with*
356 *concretions and spherulites under PPL and CPL, respectively. D) Interpreted mineralogical*
357 *QEMSCAN analysis of the thin-section shown in B and C. The main mineralogies are*
358 *indicated. The sample consists for >90% of calcite. Iron oxides occur along the laminae and*
359 *at the contact between spherulites and concretions. Pyrite occurs inward of the concretions.*
360 *Apatite is observed related to fossil fragments in the matrix. E), F) and H) Micro-petrographic*
361 *image of agglomerative spherulite in PPL, CPL and CCL, respectively.*

Table 2: Mineralogical results (wt%) of representative samples of the different lithologies.

	Representative sample of:	Carbonate laminite – spherulitites matrix	Shaly spherulitite matrix	Shaly spherulitite matrix with ostracods	Spherulites
Mineralogy (%)	Quartz	0.1	7.3	1.4	0.4
	K-feldspar		1.5		
	Calcite	91	3.2	76.2	98.6
	Dolomite/Ankerite	0.1	0.1		
	Siderite	4.8	0.2	0.2	0.3
	Goethite	1.4	5.4	1.7	0.7
	Apatite	0.5		<1%	
	Gypsum		2.4	4.0	
	Total clay	0.8	51.0	2.9	0.0
	Kaolinite		2.2		
	Interstratified I-S		46.2	2.9	
	Chlorite		2.6		
TOC (%)		~2	25-32	15-23	0.3-1.2

4.3 Organic matter

The high TOC values stimulated an in-detail characterization of the organic matter in the shaly spherulitite samples. Organic particles are composed of smaller, dispersed huminites and isolated inertinites, occurring as inertodetrinite and fusinite (Fig. 6A and B). The huminite particles show an average random reflectance of 0.32% (n = 72, st. dev. = 0.07), indicating a low thermal maturity of the Araripe spherulite samples. Very abundant are fishbones and calcious faunal remnants (Fig. 6C). The fishbones show an association with apatite (Fig. 6D). There are some organic particles observed which can be interpreted as zooclasts. These share similar petrographic features and are characterized by their roundish shape which shows a high reflection similar to that of the inertinite (Fig. 6E and F). In most cases, the cavities enclosed by them are filled with a substance petrographically similar to solid bitumen (Fig. 6E). This substance shows a low reflectivity that similar to the huminites (VR_r = 0.29%, n = 47, st. dev. = 0.06). The exact origin of these particles, which are typical for the samples investigated,

requires further research. The observation of the samples in fluorescence mode allows for the better visualization of macerals of the liptinite group (Fig. 6G and H). The high contents of lamalginite, finely distributed in between the clay layers, are typical for lacustrine organic-rich sediments (Fig. 6H). Their dominant occurrence may be the main reason for the high TOC values of the samples. Sporinites (Fig. 6H) are occasionally found, as huminite and inertinite representing an aeolian input of higher land plant material.

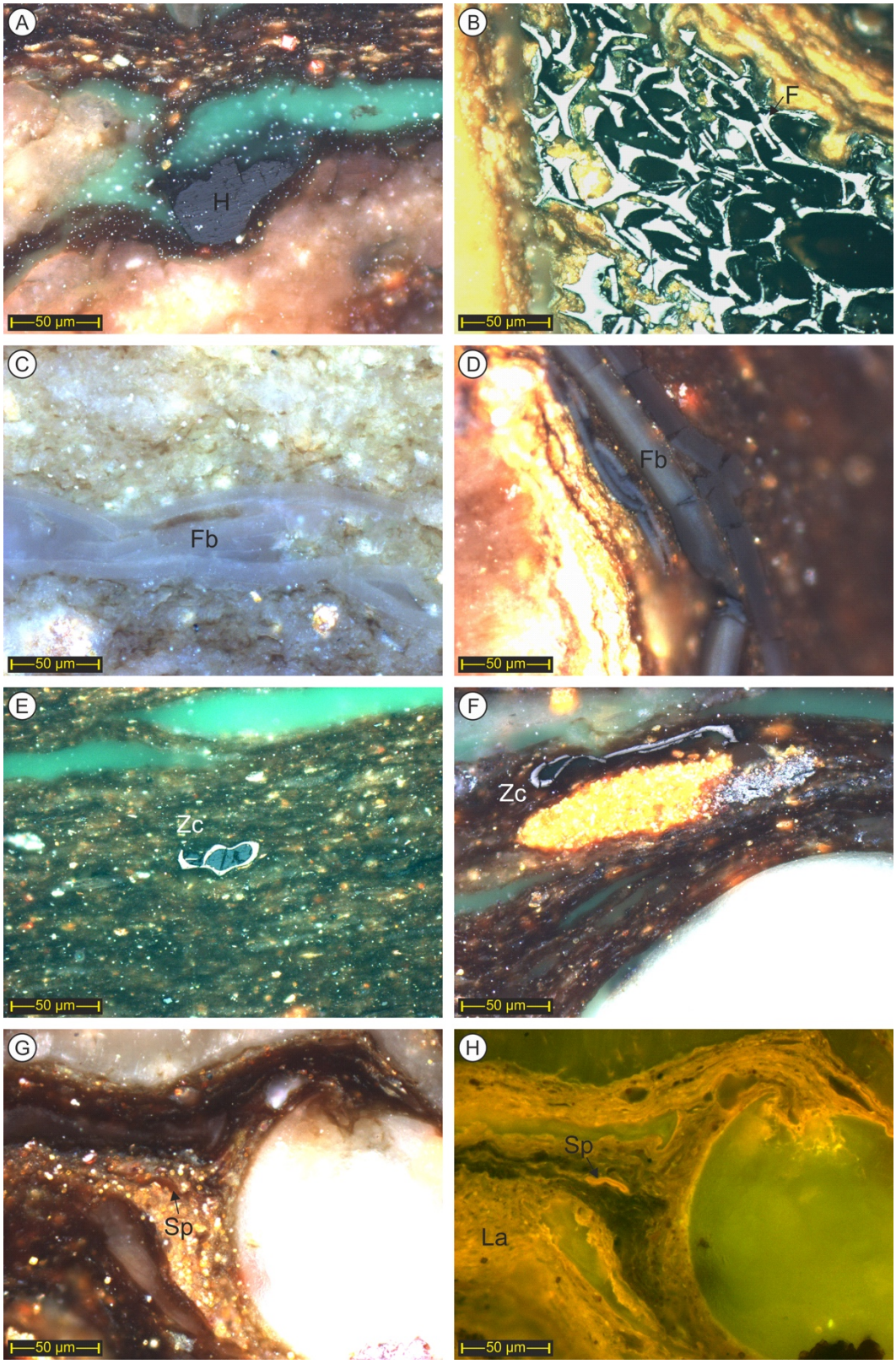

384

385 *Figure 6: Microphotographs focusing on the organic matter of the spherulites taken in*

386 *incident white (A-G) and blue light (H). H = huminite, F = fusinite, Fb = fishbone, Zc =*

387 *zooclasts, La = lamalginite, Sp = sporinite. See text for further information.*

5. Discussion

5.1 Spherulite formation

Spherulites form in a variety of depositional environments, from soil (e.g. Verrecchia et al., 1995) to travertine (e.g. Pentecost, 2005; Chafetz et al., 2018) to cave (e.g. Self and Hill, 2003) to lake (e.g. Mercedes-Martín et al., 2017; Bischoff et al., 2020) and even reef settings (e.g. Sun et al., 2017). They are explained to form by microbial mediation (e.g. Verrecchia et al. 1995; Mercedes-Martín et al., 2016; Kirkham and Tucker, 2018; Wu et al., 2020) but also an abiotic origin has been proposed (e.g. Monaghan and Lytle, 1956; Oppenheimer, 1961; Verrecchia et al., 1995; Tosca and Wright, 2015). Depending on the formation processes and the conditions during formation, spherulite fabrics and/or organization will differ (e.g. Wright and Barnett, 2020 and Mercedes-Martín et al., 2021). Although their size and fabrics can reveal a lot about the formation processes, it is equally important to consider the matrix surrounding the spherulites. A common point for spherulite formation seems to be the growth in viscous media, where crystallization is slow (Tracy et al., 1998b). Although a viscous medium is strictly not a prerequisite, it strongly catalyzes spherulite growth (Beck and Andreassen, 2010; Shtukenberg et al., 2012). Bella and Garcia-Ruiz (1987), for example, reported on spherical growth in gel. Experiments point out that the growth of spherulites from solution happens when Mg^{2+} and SO_4^{2-} are present. When either ion is absent, rhombohedra form (Tracy et al., 1998a). Thus chemistry and viscosity of the medium are considered to represent key parameters in spherulite formation, and leave their traces in the fabrics during lithification (e.g. Wright and Barnett, 2020).

In lacustrine settings several formational models are suggested (Gomes et al., 2020a), i.e. deposition in the water column or at the sediment water interface (Mercedes-Martin et al., 2017; Chafetz et al., 2018), or syndepositional to early diagenetic below the sediment-water interface (Dorobek et al., 2012; Saller et al., 2016; Wright and Barnett, 2019). In the latter case,

413 their formation requires the sediments to be still in an unconsolidated state (e.g. Herlinger et
414 al., 2017; Gomes et al., 2020a).

415 The Aptian Barabalha spherulites display a large range of sizes even within a sample,
416 so no sorting processes were involved. This would also conflict with the hydrodynamic energy
417 needed and their presence in very fine-grained sediments. In addition, they occur in a clayey
418 organic-rich matrix with the platy Mg-rich clay mineral and organic matter rich layers bended
419 around the spherulites. Occasionally the spherulites even show compromised growth or lateral
420 transition into crustiform calcites. Sulfate present as gypsum could be, given the at least
421 temporary evaporitic conditions, primary or could be secondary, related to weathering of
422 pyrite. Furthermore, samples rich in ostracods show spherulites that encapsulated some of the
423 ostracods, thus the latter were present before spherulite growth. The whole assembly of these
424 characteristics strongly point to a kind of chemically-driven concretionary/nodular radial
425 growth around ostracods or micritic cores enabled by a viscous matrix or gel formed by organic
426 matter from algae and clay or a precursor (Fig. 7). Pyrite and their weathered iron oxide
427 equivalents are found inside the spherulites, but mainly concentrated at the spherulite-matrix
428 interface, indicating a displacive growth. Although the clays do not show the typical autigenic
429 cementation textures, based on their occurrence as films contouring ostracodes and spherulites,
430 their formation is interpreted as in-situ, mimicking the depositional orientation, i.e. lamination,
431 of their precursor (similar to Wright and Barnett, 2020). Due to the spherulite growth, plate
432 minerals were pushed aside, but probably differential compaction between the matrix and
433 spherulites during burial emphasized their anastomosing morphologies (Fig. 7).
434

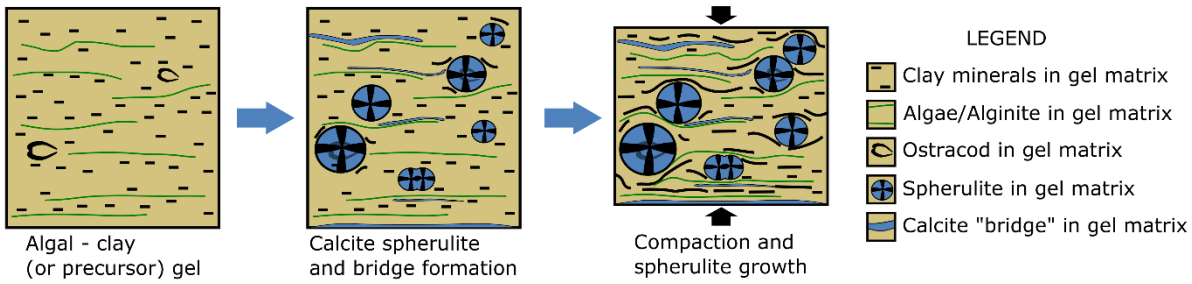

435

436 *Figure 7: Calcite spherulite and brige formation in an algal – clay viscous matrix. Ostracods*
437 *can act as nucleation site. Due to the spherulite growth, plate minerals are pushed aside.*
438 *Differential compaction between the matrix and spherulites during burial emphasized their*
439 *anastomosing morphologies. Modified from Wright and Barnett (2017). Note also the*
440 *similarities with Herlinger et al. (2017). Of importance is that these authors consider*
441 *spherulite formation in the complete absence of organic matter.*

442

443 Similarities to the Pre-Salt spherulites are striking. The Barra Velha spherulites, unless
444 reworked, occur in two "*in-situ*" associations: loosely packed in Mg-silicate matrices and in
445 floatstone textures with the spherulites surrounded by porous matrices. The pores resemble
446 fenestrae, but are associated with dolomite bridges that mimic the shapes and orientations of
447 clay plates wrapped around grains (Wright and Barnett, 2017; 2020). While the latter authors
448 observed diagenetic dolomite bridges with a clay resemblance, in the Barbalha samples we
449 observe calcite bridges and the clays are still well-preserved (Figs. 2, 3 and 7). Wright (2012),
450 Tosca and Wright (2015) and Wright and Barnett (2020) consider a Mg-silicate gel as the
451 viscous medium in which the spherulites formed, that by lithification turns into Mg-silicates.
452 Dissolution of these Mg-silicates in turn could have been the cause of a significant part of
453 secondary porosity development in the Barra Velha carbonates (Tosca and Wright, 2015). The
454 clays in the Araripe spherulites are dominantly interstratified illite – montmorillonites and thus
455 differ from the tri-octahedral stevensites reported by Tosca and Wright (2015). Despite the
456 unique abundance and significance of stevensite, several other clay types have been found in

457 Pre-Salt subsurface reservoirs, e.g. kerolite-smectites and illite-smectites (Herlinger et al.,
458 2017; Antonio, 2019). Tri-octahedral Mg-silicate stevensite (Abrahao and Warme, 1990) forms
459 from Mg-rich lake waters with a pH >9 (Jones, 1986) and with possible magmatic
460 hydrothermal activity (e.g. Tosca and Wright, 2015; Lima and De Ros, 2019). Montmorillonite
461 and illite form in basins surrounded by rocks rich in Mg^{2+}, Ca^{2+} and Fe^{2+} providing stagnant
462 (reducing) alkaline water conditions under evaporative conditions, whereby illite forms under
463 alkaline conditions and montmorillonite at even higher pH values (Reeves, 1968). For both
464 cases, high pH conditions thus prevailed. This is in line with growth of carbonate spherulites
465 in lacustrine conditions that has been proven to be restricted to specific pH conditions (pH 9.5-
466 11; Garcia-Ruiz, 1998).

467 The high TOC of the spherulite matrix of the Barbalha spherulites differs from the
468 observations for the Pre-Salt. The oil-prone alginate, however, would contribute to the
469 hydrocarbons charging the reservoir (see also Schoellkopf and Patterson, 2000; Saller et al.,
470 2016 and Spigolon et al., 2015). Given that hydrocarbon formation will be associated with
471 carboxylic and other acids, decay of organic matter could explain part of the high secondary
472 porosity in some of the Pre-Salt spherulites. For sure for the Barbalha spherulites, the organic
473 matter contributed to the viscous medium in which the spherulites precipitated. Although that
474 Tutolo and Tosca (2018) suggested that neither elevated concentration of organic acids, nor
475 biological mediation, nor a gel matrix are required for calcite spherulites, Mercedes-Martin et
476 al. (2016) show that the simplest mechanism to deposit significant spherical-radial calcite
477 bodies is to begin with a strongly supersaturated solution that contains specific but
478 environmentally common organic acids. Organic substances can lower the kinetic thresholds
479 for nucleation, while maintaining a constant supersaturation during spherulite growth
480 (Mercedes-Martín et al., 2021). In addition, based on experimental work from Wu et al. (2020),
481 alginate turned out to be essential for the growth of spherulites. Bontognali et al. (2008),

considered their fine-grained cores to precipitate in Extracellular Polymeric Substances (EPS). Spherulites, in particular those with micritic nuclei, are suggested to have been nucleated by microbial mediation (e.g. Chafetz et al., 2018). Honeycomb textures were observed by SEM in the spherulite cores and plenty of alginate was observed in the rock matrices. Spherical shapes can be produced with or without the presence of bacterial cells within a gel medium (Chekroun et al., 2004; Turner and Jones, 2005), which in the Barbalha spherulites to large extent relates to EPS from algae, in line with experimental work from Wu et al. (2020) and Mercedes-Martín et al. (2021). Wright and Barnett (2017) pointed out that spherulitic carbonates are common features in microbial mats but are several orders of magnitude smaller than those seen in the Barra Velha (Sanchez-Navas et al., 2009; Spadafora et al., 2010; Wanas, 2012). A decreased spherulite size could be related to increased salinities (Mercedes-Martín et al., 2021). However, large-sized spherulites are observed in the Aptian Barabalha samples (Batateira bed) as discussed in this study. Even though their spherulite nucleation started from irregular grains or as tiny spheres in the organic-rich matrix, they resulted in very well-rounded, up to cm-scaled spherulites. In addition, Meister et al. (2011) show that calcite spheres, similar to those of the Araripe Basin and the Pre-Salt, only form from a solution with organic matter present, while spherical precipitation in abiotic experiments resulted in aragonite. Furthermore, not only the spheres but also the clays could have partially formed from the viscous medium rich in EPS (Fig. 7). Bischoff et al. (2020) also show the essential presence of EPS both in the formation of Mg-Si precipitates as well as for high-Mg calcite spherulites. In conclusion, the observations from the Batateira spherulititesuggest that instead of considering microbial and clay or silica gel mediation as opposing theories, they should rather be considered as complimentary and/or cooperative in the genesis of spherulites. Considering the abiotic versus biotic formation, the presence and catalyzing effect of the alginate matrix is undeniable for the Barabalha spherulites.

5.2 Water depth

5.2.1 *Extra-spherulitite facies information*

Often lateral and vertical facies changes are used to interpret changes in the depositional system, including water depth. The abrupt transition from fluviatile deposits to spherulite-bearing lacustrine lithologies is, however, structurally controlled. Scherer et al. (2015) considered epeirogenetic regional movements as part of the sag basin during the post-rift stage responsible for the rapid increase in subsidence and creation of accommodation space. This resulted in a sudden relatively deep depression, with continued freshwater supply, most likely fed by the formerly existing river system. Renewed tectonic activity resulted in a very significant change in the drainage regime, base level, or both, resulting in an erosive unconformity and therefore a temporarily interrupted lake system (Assine et al., 2014; Fambrini et al., 2019). After a temporal riverine system, again a more persistent lacustrine system established that transitioned into the lacustrine carbonates of the Crato Formation, the main lacustrine phase in the Araripe Basin.

The transition from the upper lacustrine phase of the Barbalha formation towards the Crato laminites, consequently, is continuous and so the latter might hold crucial information regarding the water depth of the paleo-lake. In addition, the laminites possibly represent a better-exposed occurrence of the laminites observed as part of the Batateira beds. Thirdly, the oil shale facies with dark clay/organic-rich layers and nodular carbonates (Neumann et al., 2003; their Fig. 5) or nodular microfacies (Catto et al., 20016; their Fig. 6) or limestone with organic laminae (Cabral et al., 2019; their Fig. 6) might represent later occurring spherulite events as part of the Crato lacustrine system.

However, as summarized by Martill et al. (2007) the Crato paleo lake water has been considered as fresh (Maisey, 1990; 1996), hypersaline (Martill and Wilby, 1993) or brackish

(Bechly, 1998; Neumann et al., 2003) and the water depth as both, shallow (Maisey, 1990; Warren et al., 2017) and relatively deep (Martill and Loveridge, 2006). The depositional setting has been referred to as a lake or a lagoon (Martill, 1993), closed, or with a connection to the ocean in an epeiric sea setting (Arai, 2000; Assine et al., 2016, Varejao et al., 2016). Martill et al. (2007) and Barling et al. (2020) relate the remarkably low abundance of sedimentary patterns in the laminites to deposition below the storm wave base, i.e. to a water depth of 50 - 200 m. Martill et al. (2008) was more careful in his conclusions stating it was "probably more than 30 m". Varejão et al. (2020) highlight the importance on focusing on separate intervals of the Crato Formation, since they reflect changing water levels and hydrological connections. Considering that the Crato *Konservat-Lagerstätte* laminites are found across the Araripe Basin (~8000 km^2) and based on a comparison of the maximum water depths of present-day saline analogue lakes (Table 3), suggests that the deepest water depth of the lake was at least 20 m. The large areal extension, however, also implies that most of it (i.e. average water depth; Table 3) most likely must have been more shallow. Studies by Catto et al. (2016), Warren et al. (2017) and Varejao et al. (2019) interpret the association of stromatolites with halite hoppers, Kinneyia wrinkles, pseudo-columns, domes, MISS, thrombolites, preserved microbial mats, oncoids and breccias in the *Konservat-Lagerstätte* interval of the Crato Formation as shallow-water conditions (<10 m depth). While the Crato laminites are geographically continuous over the entire Araripe Basin (Fabin et al., 2018), with a minimum NW-SE extent of ~70 km (Heimhofer et al., 2010), the spherulite Batateira beds are known to be laterally continuous at distances most likely just above 20 km (Scherer et al., 2015). The reduced lake size and the fact that tectonic events were able to quickly change between the Barbalha lake and riverine setting, suggest a more shallow water depth compared to the Crato laminites, i.e. maximum water depth ~ 10 m. The average water depth consequently most likely was <10m.

Table 3: Non-exhaustive overview of (hyper)saline lake dimensions at arbitrary moments. These data gathered from several sources (see reference column in addition to Wikipedia) should be considered critically, especially given the strongly varying sizes of these lakes, with many of them being remnants of larger lakes.

	Length (km)	Width (km)	Surface (km^2)	Average depth (m)	Max depth (m)	References:
Owens lake (U.S.A.)	28	16	451		0.91	Benson et al., 1996; Bacon et al., 2018
Dead Sea (Israel - Jordan)	50	15	605	199	298	Nof et al., 2012
Salton sea (U.S.A.)			889		13	Doede et al., 2020
Lago Cuitzeo (Mexico)	20	20	350	27	27	Mendoza et al., 2006
Lake Corangamite (Australia)			234	5	7	Williams, 1995; Tweed et al., 2009
Lake Poopó (Bolivia)			1000	1	2	Zola et al., 2006
Great Salt Lake (U.S.A.)	120	45	4400	4.9	14	Null and Wurtsbaugh, 2020
Lake Urmia (Iran)	140	55	5200		16	Schulz et al., 2020
Aral Sea (Kazakhstan - Uzbekistan)			17160	10	40	Burr et al., 2019
Ebi lake (China)			1070	1.4	2.8	Zhou et al., 2019
Lake Assal (Afar depression)	19	6.5	54	7.4	>40	Pérez and Chebude, 2017
Lake Abert (U.S.A.)	24	11	170	1.5	3.4	Senner et al., 2018
Mono lake (U.S.A.)	21	15	183	17	48	Hodelka et al., 2020
Lake Walker (Canada)	33	<10			280	Benson et al., 1991
Lake Chad (Nigeria - Niger -	50	30	1540	1.5	11	Pham-Duc et al., 2020

Chad - Cameroon)						
Lake Bogoria (Kenya)		3.5	36		12	Renaut et al., 2017; Kiage et al., 2020
Lake Nakuru (Kenya)	12	10	55	0.3	1.8	Kiage et al., 2020
Lake Elementaita (Kenya)			21		<1	Kiage et al., 2020

561 5.2.2 *Intra-spherulitite facies information*

562 The illite – montmorillonites of the spherulitite matrices are known to accumulate in
563 low energy settings, not prone to exposure, desiccation or reworking. The relatively low quartz
564 and feldspar contents corroborate the low contribution of detritals. In addition, the
565 accumulation of organic matter is characteristic for low(er)-energy sub- to anoxic depositional
566 areas within the lake. Lacustrine carbonates alternating with montmorillonite and illite clays,
567 and containing evaporites are diagnostic for closed, chemically stratified, saline lakes in a semi-
568 arid environment (Reeves, 1968). Because high-water level stages would have favored thermal
569 water stratification and organic matter preservation, these factors can support a ´deep´
570 depositional scenario below the wave base. Alternatively, shallow restricted bays or lagoons
571 could also provide the required low energetic conditions. Microbial mats in the photic zone
572 independent of water depth can provide anoxic conditions due to internal stratification (as
573 reported by Varejao et al., 2019 and Barling et al., 2020 for the Crato Formation).
574 Perforations/borings into the spherulites (Fig. 3K) requires their formation to take place before
575 substantial burying and in sufficiently shallow water conditions. In addition, the presence of
576 gypsum and pyrite in the spherulite-bearing lithologies is an indication of shallow water
577 conditions. The iron oxides (next to pyrite) at the spherulite-matrix contact are indeed
578 interpreted as alteration products of pyrite. Concentric enrichment of pyrite has previously been
579 reported from carbonate concretions in organic carbon-rich mudrocks (Caleman and Raiswell,
580 1995) and are thought to reflect the activity of sulfate-reducing bacteria at shallow depth in

non-lithified sediments (Heimhofer et al., 2017). Anoxic conditions are ideal for pyrite formation via bacterial sulphate reduction when sulfates are present.

Relatively high C/N values at constant $\delta^{13}C_{org}$ of the organic rich spherulites (Table 1), suggest denitrification (possibly associated to an Oceanic Anoxic Event – OAE; similar to Bastos et al., 2020), typical for low oxygen hypolimnetic waters or bottom sediments. $\delta^{18}O$-$\delta^{13}C$ signals are a function of the geographical and climatic setting, hydrology and the history of the waterbody (Talbot 1990). The relatively low $\delta^{18}O$ of the studied spherulitites should not be surprising given the freshwater input from the fluvial/deltaic systems related to the fast tectonic transition. The low $\delta^{13}C$ of the spherulitites could be related to the high organic matter content, at least if the latter got oxidized and dissolved. Not only the matrix containing the low $\delta^{13}C$ organic matter, but also the calcite spherulites show low $\delta^{13}C$ signatures (Table 1). This can be related to water aging (Holmden et al., 1998), which is greatest in shallow, poorly circulated waters (Immenhauser et al., 2003), in line with the extra-facies arguments for a lake with a depth below 10m, at least at the time of spherulite formation.

5.3 Araripe Basin - South Atlantic paleo-connection?

Similarities with deposits from adjacent Basins have often been the cause for proposing a marine ingression into the Araripe Basin. Arai (2000), based on the presence of dinoflagelates, stated that a global eustatic sea-level rise in the late Early Cretaceous resulted in the episodic establishment of a highly restricted NW-SE trending epeiric seaway linking the intracratonic Araripe Basin either with the opening of the northern part of the South Atlantic Ocean (via the Reconcavo, Tucano and Jatoba Basin complex) or the Central Atlantic Ocean (via the Parnaiba or Potiguar basins). For the Ipubi and Romualdo Formations this connection to the sea has been confirmed based on paleontological and geochemical data (Dias-Brito, 1992, 2000; Azevedo 2001, 2004; Rodrigues et al., 2020; Melo et al., 2020), but for the

606 Barbalha and Crato Formations, it has been an ongoing topic of debate. Arai (1999, 2011, 2012,
607 2014) found marine forms of foraminifera and dinoflagellates in the Crato Formation, and
608 together with radiolaria, molluscs, echinoids, crustaceans and fishes from other Brazilian
609 continental Basins invokes a Tethyan connection. Assine et al. (2016) replying to Arai (2014)
610 emphasized the necessity of a multidisciplinary approach and pointed out the critical role of
611 the Araripe Basin in the evaluation of an interbasinal paleo-connection. Stratigraphic and
612 paleocurrent data indicate three different large-scale drainage basins in the northeast of Brazil,
613 implying a marine ingression from the SE for the Araripe Basin via the Tucano and Jatobá
614 Basins (Assine et al., 2016). Although Arai (2016) rejected the drainage scenario, both agree
615 on the connection between the Araripe, Tucano and Jatobá Basins. Varejão et al. (2016)
616 confirmed the presence of the Crato Formation, or at least very similar deposits, in the Tucano
617 Basin and at inselbergs in the Jatobá Basin. They show the same paleo-drainage flow, i.e. south
618 to the South Atlantic Ocean (or giant lake at that time), also in line with the paleoflow of the
619 Barbalha Formation (Assine et al., 2014, Scherer et al., 2015; Fambrini et al., 2019). Varejão
620 et al. (2016, 2019) confirm the presence of the undulated laminites but also the so-called
621 "nodular laminites" containing spherulites in the North Tucano Basin. Varejão et al. (2019)
622 described calcite spherulites in the shallow water Amargosa Beds which are stratigraphically
623 correlated to the Batateira Beds. In this way, paleontological, paleo-current and lithofacies data
624 all seem to support either a connection along the different basins or the similarity in
625 depositional environments across the basins and emphasize the strategic importance to look for
626 onland equivalents of the Pre-Salt deep reservoir units.
627
628 *5.4 Biotic influence before, during and after Barbalha spherulite formation*
629 Providing evidence of biotic influence on mineralization processes remains one of the
630 biggest challenges in geology. Summarizing all the petrographic evidence of the Barbalha

spherulitites, however, reveals the biotic influence before, during and after spherulite formation. As evidenced by the well-preserved lamalginate organic matter, microbial mats and/or their biopolymers accumulated. These mats and biopolymers kinetically accelerated calcite nucleation and sustained supersaturation for continued spherulite growth, as also confirmed from laboratory experiments (Mercedes-Martín et al., 2021). The different type of substrates and their composition suggest that nucleation was governed by chemically suitable substrates, e.g. calcite fragments, ostracods and other shells, and/or ionic concentration in organic matter, often preserved as micrite peloids (e.g. Riding et al., 2000). The concretionary growth by chemically-driven concentration, in essence abiotic, was mediated by the sustained supersaturation governed by the viscous mixed microbial mat - clay(-precursor) matrix. Microborings and the concentric enrichment of pyrite reveal the microbial activity after spherulite formation. Anoxic conditions, caused by the microbial mats, were ideal for pyrite formation via bacterial sulphate reduction. These spherulitites consequently represent a, perhaps atypical, example of hybrid microbial-abiotic carbonates (Riding and Virgone, 2020).

5.5 The Araripe Aptian deposits as a Pre-Salt carbonate analogue

Lake deposystems are often controlled by highly complex hydrological factors reflecting the interaction of local climate, tectonics and the composition of the catchment geology (Wright and Rodriguez, 2018). Given that the Barbalha and geographically proximal Barra Velha and Macabu Formations are both lower Aptian deposits, they evidently possess several similarities with regard to their overall setting. The structural frame for all basins is the break-up of the Gondwana supercontinent associated with rifting and formation of horst-graben structures (Heine et al., 2013). Despite that the Pre-Salt deposits formed in the active rift basin ant that the Araripe basin developed as an intraplate intersection, they both are dominated by extension. In addition, the climatic conditions, i.e. semi-arid conditions (Doyle et al., 1982;

Lima and Perinotto, 1983; Ziegler et al., 2003), were the same. As such, not only the Araripe rock archive but also deposits in other inland basins, e.g. the Codo Formation (Bahniuk et al., 2005), can be considered as analogues. Dias (2005) described an epicontinental sea with a high continental influence and coastlines sectioned by valleys where in embayments, hypersaline, microbial communities formed microbialites. It is possible that temporarily or permanently connected volcanically influenced lakes in this rift setting are surrounded by the same rock types. The Barbalha (and Crato and Codo) Formation are part of the transitional sag phase, marked by thermal subsidence and huge shallow lake generation (e.g. Pietsch et al., 2018). The Cretaceous is known worldwide for its short-term eustatic sea-level changes (Ray et al., 2019). Large-scale marine ingressions were occasional (Silva-Telles et al., 1994; Althaus et al., 2019; Rodrigues et al., 2020) and are recognized within these basins during the early Aptian (e.g. Crato Formation) but also for the overlying evaporites (Ipubi Formation in the Araripe Basin). The Barbalha laminites and spherulites are remarkably similar when comparing with Pre-Salt data and descriptions , not only to those reported on the Brazilian side of the South Atlantic but also in their West-African counterparts (Examples of spherulites in e.g. Herlinger et al., 2017; Farias et al., 2019; Lima and De Ros, 2019 and Wright and Barnett, 2020). Organic-rich mudstones, some with significant amounts of ostracods are reported, for example from the Kwanza deposits and are even considered the main source rocks in Pre-Salt (Saller et al., 2016). In addition, the type I organic matter of the Araripe spherulites (see also Spigolon et al., 2015) is in line with the dominance of type I in the Pre-Salt mudrocks (Mello et al., 1994; Mello, 2006; Goldberg et al., 2017).

From a geochemical view, the Araripe and South-Atlantic Pre-Salt deposits show strongly different $\delta^{18}O$ and $\delta^{13}C$ signatures (Fig. 8). While the $\delta^{13}C$ signatures of the Pre-Salt deposits are relatively constant, it should be noted that they show a high variation in $\delta^{18}O$. The nearly constant $\delta^{13}C$ can be interpreted in terms of lake water CO_2 in equilibrium with

atmospheric CO_2 (Pietsch et al., 2020). However, fractionation from magmatic CO_2, or even CO_2 resulting from dissolution of marine carbonates at ~50 °C, would result in very similar signatures (Claes et al., 2015, Fig. 21), and should be considered when interpreting the stable isotope signatures of the PreSalt deposits. Both Pre-Salt laminites and spherulites show much higher $\delta^{18}O$ signatures compared to their Araripe equivalents. These indicate a higher influence of meteoric waters both during deposition, as mentioned earlier, but also diagenesis for the Barbalha Formation. Indeed, the Araripe deposits have been exposed to meteoric alteration, recrystallisation and cementation, by which they would have inherited low $\delta^{18}O$ signatures. On the other hand, diagenetic dolomite formation and dolomitisation are known to drive the $\delta^{18}O$ to significantly higher values (e.g. McCormack et al., 2019) for varying $\delta^{13}C$. Dolomite formation is observed in the Araripe samples and some dykes were reported (Martill et al., 2008), with samples showing indeed a positive shift in $\delta^{18}O$ (Fig. 7). In the Pre-Salt deposits, separating calcite from dolomite during sampling was not possible, however, Pietsch et al., (2020) excluded the effect of mineralogy and facies on the stable isotopes. Lima et al. (2020), with supporting evidence from fluid inclusion microthermometry and radiogenic strontium isotopes, interpreted the $\delta^{18}O$-$\delta^{13}C$ signatures as altered by hydrothermal fluids, with similar depositional and diagenetic processes over a regional scale, suggesting a vast lake or lakes that were hydro-geologically connected. It is exciting to imagine that the Araripe deposits were able to maintain the more pristine geochemical signatures as opposed to the strongly diagenetically altered Pre-Salt.

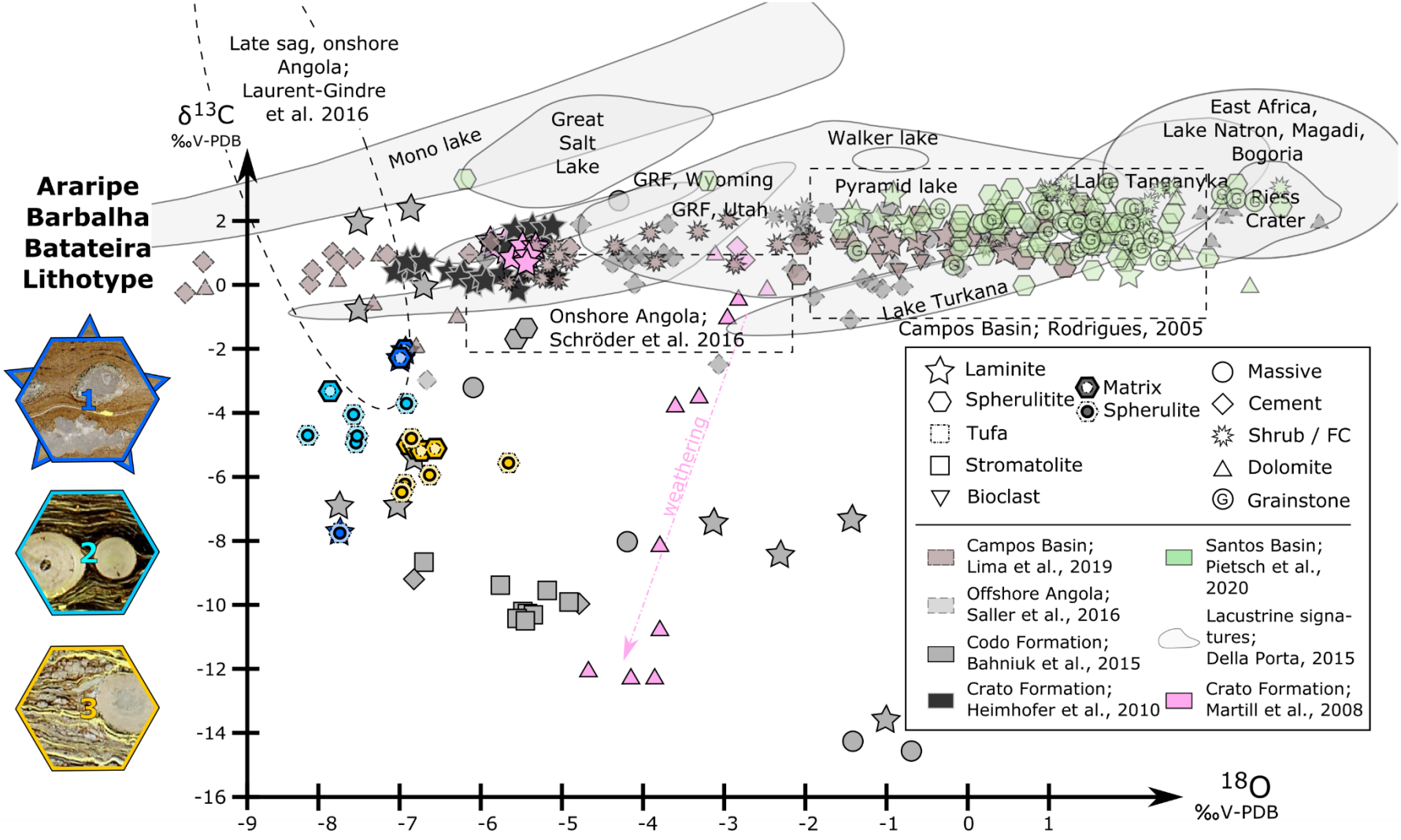
Araripe
Barbalha
Batateira
Lithotype
1
2
3
δ13C
‰V-PDB
Late sag, onshore Angola; Laurent-Gindre et al. 2016
Mono lake
Great Salt Lake
GRF, Wyoming
GRF, Utah
Walker lake
Pyramid lake
East Africa, Lake Natron, Magadi, Bogoria
Lake Tanganyka
Riess Crater
Lake Turkana
Onshore Angola; Schröder et al. 2016
Campos Basin; Rodrigues, 2005
Weathering
Laminite
Spherulitite
Tufa
Stromatolite
Bioclast
Matrix Spherulite
Massive
Cement
Shrub / FC
Dolomite
Grainstone
Campos Basin; Lima et al., 2019
Offshore Angola; Saller et al., 2016
Codo Formation; Bahniuk et al., 2015
Crato Formation; Heimhofer et al., 2010
Santos Basin; Pietsch et al., 2020
Lacustrine signatures; Della Porta, 2015
Crato Formation; Martill et al., 2008
2
0
-2
-4
-6
-8
-10
-12
-14
-16
-9
-8
-7
-6
-5
-4
-3
-2
-1
0
1
18O
‰V-PDB

703

Fig. 8: Stable $\delta^{18}O$- $\delta^{13}C$ isotopes of the lithofacies from the Barbalha Batateira deposits compared to literature data. The three lithotypes with spherulites of interest in this study are represented, including the (1) laminites with nodular spherulite and crust growth, (2) shaly organic-rich spherulitites containing spherulites with micritic cores, (3) shaly organic-rich spherulitites with a pronounced ostracod presence, also in the spherulites.

6. Conclusions

The Aptian Araripe Barbalha spherulitites form an almost time-equivalent, geographically proximal, possibly sedimentological analogue for some of the Pre-Salt spherulites. Related to the horst-graben structural setting, the influence of surrounding lithologies, lateral and vertical facies continuity, the hypersaline lacustrine depositional environment, the biotic versus abiotic formation and petrophysical characteristics, the Barbalha Formation consequently might provide insight into the Pre-Salt reservoir rocks.

Based on the lithological characteristics of the Barbalha spherulites, information of surrounding lithologies and comparison with other lakes, the water depth of the paleolake at that time was less than 10 meter.

The presence of spherulites in organic, clay-rich lacustrine Aptian Araripe laminites suggests that microbial and clay mediation were complimentary processes in the genesis of the spherulites. Their nodular/concretionary growth encapsulated particles like e.g. ostracodes but acted displacively for sulfides and plate minerals.

The potential paleo-connection or at least similar depositional environments of the onland basins compared to the South Athlantic strengthen their use as analogues for depositional and early diagenetic conditions. However, important differences, for example with

regard to stable isotope geochemistry, should be further elucidated, taking into account the strongly contrasting diagenetic overprints.

7. Acknowledgements

This project has been partially subsidized through the ERANET Cofund ACT (Project no. 271497), the European Commission, the Research Council of Norway, the Rijksdienst voor Ondernemend Nederland, the Bundesministerium für Wirtschaft und Energie, and the Department of Business, Energy & Industrial Strategy, UK.

8. References

Abrahao, D. and Warme, J.E., 1990. Lacustrine and Associated Deposits in a Rifted Continental Margin--Lower Cretaceous Lagoa Feia Formation, Campos Basin, Offshore Brazil: Chapter 18.

Althaus, C.E., dos Santos Scherer, C.M., Kuchle, J., dos Reis, A.D., Ferronatto, J.P.F., De Ros, L.F. and Bardola, T.P., 2020. Wave-dominated lacustrine margin of Aptian pre-salt: Mucuri Member, Espírito Santo Basin. Journal of South American Earth Sciences, 99, p.102490.

Alvarenga, R.S., Iacopini, D., Kuchle, J., Scherer, C.M.S. and Goldberg, K., 2016. Seismic characteristics and distribution of hydrothermal vent complexes in the Cretaceous offshore rift section of the Campos Basin, offshore Brazil. Marine and Petroleum Geology, 74, pp.12-25.

do Amarante, F.B., Kuchle, J., Iacopini, D., dos Santos Scherer, C.M., dos Santos Alvarenga, R., Ene, P.L. and Schilling, A.B., 2020. Seismic tectono-stratigraphic analysis of

754 the Aptian pre-salt marginal system of Espírito Santo Basin, Brazil. Journal of South American
755 Earth Sciences, 98, p.102474.
756
757 Arai M. 1999. A transgressão marinha mesocretácea: sua implicação no paradigma da
758 reconstituição paleogeográfica do Cretáceo no Brasil. In: 5º Simpósio sobre o Cretáceo no
759 Brasil, v. Boletim, p.577-582.
760
761 Arai, M., Neto, J.B., Lana, C.C. and Pedrão, E., 2000. Cretaceous dinoflagellate
762 provincialism in Brazilian marginal basins. Cretaceous Research, 21(2-3), pp.351-366.
763
764 Arai M. 2011. Paleogeografia do Atlântico Sul no Aptiano: um novo modelo a partir
765 de dados micropaleontológicos recentes. Boletim de Geociências da Petrobras, 17: pp.331-351.
766
767 Arai, M., 2012. Evidência micropaleontológica da ingressão marinha aptiana (pré-
768 evaporítica) na Bacia do Araripe, Nordeste do Brasil. In 46 Congresso Brasileiro de Geologia.
769
770 Arai, M., 2014. Aptian/Albian (Early Cretaceous) paleogeography of the South
771 Atlantic: a paleontological perspective. Brazilian Journal of Geology, 44(2), pp.339-350.
772
773 Arai, M., 2016. Reply to the comments of Assine et al.(Comments on paper by M. Arai"
774 Aptian/Albian (Early Cretaceous) paleogeography of the South Atlantic: a paleontological
775 perspective"). Brazilian Journal of Geology, 46(1), pp.9-13.
776
777 De Araújo, C.C., Moretti, P.A., Madrucci, V., da Silva, N.C., Toczeck, A. and Almeida,
778 A.B., 2012. Pre-salt facies in the Carmopolis area, Northeast Brazil: stratigraphy and

779 depositional model. American Association of Petroleum Geologists, Tulsa, OK, Search and
780 Discovery, article, 50544, pp.193-249.
781
782 Assine, M.L., Quaglio, F., Warren, L.V. and Simões, M.G., 2016. Comments on paper
783 by M. Arai" Aptian/Albian (Early Cretaceous) paleogeography of the South Atlantic: a
784 paleontological perspective". Brazilian Journal of Geology, 46(1), pp.3-7.
785
786 Awramik, S.M. and Buchheim, H.P., 2015. Giant stromatolites of the Eocene Green
787 River Formation (Colorado, USA). Geology, 43(8), pp.691-694.
788
789 Azevedo R.L.M. 2001. O Albiano no Atlântico Sul: estratigrafia, paleoceanografia e
790 relações globais. PhD Thesis, Instituto de Geociências, Universidade Federal do Rio Grande
791 do Sul, Porto Alegre, 401 p.
792
793 Azevedo R.D. 2004. Paleoceanografia ea evolução do Atlântico Sul no Albiano.
794 Boletim de Geociências da Petrobras, 12: pp.231-249.
795
796 Bacon, S. N., Lancaster, N., Stine, S., Rhodes, E., & Holder, G. A. M. (2018). A
797 continuous 4000-year lake-level record of Owens Lake, south-central Sierra Nevada,
798 California, USA. Quaternary Research.
799
800 Bahniuk, A.M., Anjos, S., França, A.B., Matsuda, N., Eiler, J., McKenzie, J.A. and
801 Vasconcelos, C., 2015. Development of microbial carbonates in the Lower Cretaceous Codó
802 Formation (north-east Brazil): Implications for interpretation of microbialite facies
803 associations and palaeoenvironmental conditions. Sedimentology, 62(1), pp.155-181.

Barling, N., Martill, D.M., Heads, S.W. and Gallien, F., 2015. High fidelity preservation of fossil insects from the Crato Formation (Lower Cretaceous) of Brazil. Cretaceous Research, 52, pp.605-622.

Barling, N., Martill, D. M., and Heads, S. W., 2020. A geochemical model for the preservation of insects in the Crato Formation (Lower Cretaceous) of Brazil. Cretaceous Research, 104608.

Bastos, L.P.H., Pereira, E., da Costa Cavalcante, D., Alferes, C.L.F., de Menezes, C.J. and Rodrigues, R., 2020. Expression of Early Cretaceous Global anoxic events in northeastern Brazilian basins. Cretaceous Research, p.104390.

Batten D.J. 2007. Spores and pollen from the Crato Formation: biostratigraphic and palaeoenvironmental implications. In: Martill D.M., Bechly G., Loveridge RF. (eds.), The Crato Fossil Beds of Brazil: Window into an Ancient World. Cambridge, Cambridge University Press, p. 566-573.

Beck, R., & Andreassen, J. P., 2010. Spherulitic growth of calcium carbonate. Crystal Growth & Design, 10(7), 2934-2947.

Benson, L. V., Meyers, P. A., & Spencer, R. J. (1991). Change in the size of Walker Lake during the past 5000 years. Palaeogeography, Palaeoclimatology, Palaeoecology, 81(3-4), 189-214.

Benson, L. V., Burdett, J. W., Kashgarian, M., Lund, S. P., Phillips, F. M., & Rye, R. O. (1996). Climatic and hydrologic oscillations in the Owens Lake Basin and adjacent Sierra Nevada, California. Science, 274(5288), 746-749.

Bertolini, A.C., Monteiro, J., Canas, J.A., Betancourt, S.S., Mullins, O.C., Colacelli, S. and Polinski, R.K., 2019, March. Reservoir Fluid Geodynamics in Brazilian Presalt Carbonate Field. In SPE Middle East Oil and Gas Show and Conference. Society of Petroleum Engineers.

Bechly, G., 1998. New fossil dragonflies from the Lower Cretaceous Crato Formation of north-east Brazil (Insecta: Odonata): Stuttgarter Beiträge zur Naturkunde.

Belila, A.M.P., Basso, M., Chinelatto, G.F., Kuroda, M.C. and Vidal, A.C., 2020. Pore typing using nuclear magnetic resonance, an example with samples from cretaceous pre-salt lacustrine carbonates in the Santos Basin, Brazil. Journal of Petroleum Science and Engineering, p.107079.

Bella, S.D. and Garcia-Ruiz, J.M., 1987. Banding structures in induced morphology crystal aggregates of $CaCO_3$. Journal of Materials Science, 22(9), pp.3095-3102.

Berthou P.Y., Depeche F., Colin J.P., Filgueira J.B.M., Teles M.S.L. 1994. New data on the ostracods from Crato lithologic units (lower member of the Santana Formation, Latest Aptian- Lower Albian) of the Araripe Basin (Northeastern Brazil). Acta Geologica Leopoldensia, 39(2):539-554.

Bischoff, K., Sirantoine, E., Wilson, M. E., George, A. D., Mendes Monteiro, J., & Saunders, M., 2020. Spherulitic microbialites from modern hypersaline lakes, Rottnest Island, Western Australia. Geobiology.

Bontognali, T.R., Vasconcelos, C., Warthmann, R.J., Dupraz, C., Bernasconi, S.M. and McKenzie, J.A., 2008. Microbes produce nanobacteria-like structures, avoiding cell entombment. Geology, 36(8), pp.663-666.

Bouton, A., Vennin, E., Pace, A., Bourillot, R., Dupraz, C., Thomazo, C., Brayard, A., Désaubliaux, G. and Visscher, P.T., 2016. External controls on the distribution, fabrics and mineralization of modern microbial mats in a coastal hypersaline lagoon, Cayo Coco (Cuba). Sedimentology, 63(4), pp.972-1016.

Burr, G. S., Kuzmin, Y. V., Krivonogov, S. K., Gusskov, S. A., & Cruz, R. J. (2019). A history of the modern Aral Sea (Central Asia) since the Late Pleistocene. Quaternary Science Reviews, 206, 141-149.

Cabral, F.A.D.A., Silveira, A.C.D., Ramos, G.M.S., Miranda, T.S.D., Barbosa, J.A. and Neumann, V.H.D.M.L., 2019. Microfacies and diagenetic evolution of the limestones of the upper part of the Crato Formation, Araripe Basin, northeastern Brazil. Brazilian Journal of Geology, 49(1).

Carminatti, M., Dias, J.L., Wolff, B., 2009. From turbidites to carbonates: breaking paradigms in deep waters. In: Offshore Technology Conference, pp. 4-7. May.

Carminatti, M., Wolff, B., Gamboa, L., 2008. New exploratory frontiers in Brazil. In: 19th World Petroleum Congress. World Petroleum Council.

Catto, B., Jahnert, R.J., Warren, L.V., Varejao, F.G. and Assine, M.L., 2016. The microbial nature of laminated limestones: lessons from the Upper Aptian, Araripe Basin, Brazil. Sedimentary geology, 341, pp.304-315.

De Castro, D. L., & Castelo Branco, R. M. G., 1999. Caracterização da arquitetura interna das bacias do Vale do Cariri (NE do Brasil) com base em modelagem gravimétrica 3-D. Revista Brasileira de Geofísica, 17(2-3), 130-144.

Celestino, M.A.l., Miranda, T.S., Mariano, G., Lima, M.A., Carvalho, B.R.B.M, Falcão, T.C., Topan, J.G., Barbosa, J.A., Gomes, I.F, 2020. Fault Damage Zones Width: Implications For The Tectonic Evolution Of The Araripe Basin, Brazil. Journal of Structural Geology.

Ceraldi, T.S. and Green, D., 2017. Evolution of the South Atlantic lacustrine deposits in response to Early Cretaceous rifting, subsidence and Lake Hydrology. Geological Society, London, Special Publications, 438(1), pp.77-98.

Chafetz, H., Barth, J., Cook, M., Guo, X. and Zhou, J., 2018. Origins of carbonate spherulites: implications for Brazilian Aptian pre-salt reservoir. Sedimentary Geology, 365, pp.21-33.

Chafetz, H.S. and Guidry, S.A., 1999. Bacterial shrubs, crystal shrubs, and ray-crystal shrubs: bacterial vs. abiotic precipitation. Sedimentary Geology, 126(1-4), pp.57-74.

Claes, H., Soete, J., Van Noten, K., El Desouky, H., Erthal, M.M., Vanhaecke, F., Özkul, M. and Swennen, R., 2015. Sedimentology, three-dimensional geobody reconstruction and carbon dioxide origin of Pleistocene travertine deposits in the Ballık area (south-west Turkey). Sedimentology, 62(5), pp.1408–1445.

Claes, H., Degros, M., Soete, J., Claes, S., Kele, S., Mindszenty, A., Török, Á, El Desouky, H., Vanhaecke, F. and Swennen, R., 2017a. Geobody architecture, genesis and petrophysical characteristics of the Budakalász travertines, Buda Hills (Hungary). Quat. Int., 437, pp.107–128.

Claes, H., Erthal, M.M., Soete, J., Özkul, M. and Swennen, R., 2017b. Shrub and pore type classification: Petrography of travertine shrubs from the Ballık-Belevi area (Denizli, SW Turkey). Quat. Int., 437, pp.147–163.

Claes, H., Huysmans, M., Soete, J., Dirix, K., Vassilieva, E., Erthal, M. M., Vandewijngaerde, W., Hamaekers, H., Aratman, C., Özkul, M. and Swennen, R., 2019. Elemental geochemistry to complement stable isotope data of fossil travertine: Importance of digestion method and statistics. Sedimentary Geology, 386, 118-131.

Coleman, M.L. and Raiswell, R., 1995. Source of carbonate and origin of zonation in pyritiferous carbonate concretions; evaluation of a dynamic model. American Journal of Science, 295(3), pp.282-308.

928

929 Chekroun, K.B., Rodríguez-Navarro, C., González-Muñoz, M.T., Arias, J.M.,
930 Cultrone, G. and Rodríguez-Gallego, M., 2004. Precipitation and growth morphology of
931 calcium carbonate induced by Myxococcus xanthus: implications for recognition of bacterial
932 carbonates. Journal of Sedimentary Research, 74(6), pp.868-876.

933

934 De Boever, E., Brasier, A. T., Foubert, A. and Kele, S., 2018. What do we really know
935 about early diagenesis of non-marine carbonates? Sed. Geol., 361, pp.25-51.

936

937 Dias, J.L., 1998. Analise sedimentologica e estratigrafica do Andar Aptiano em parte
938 da margem leste do Brasil e no plato das Malvinas - consideraçoes sobre as primeiras incursoes
939 e ingressoes marinhas do Oceano Atlantico sul Meridional. Universidade federal do Rio
940 Grande Do Sul, p. 399.

941

942 Dias, J.L., 2005. Tectonica, estratigrafia e sedimentaçao no Andar Aptiano da mar-
943 gemlestebrasileira. Bol. Geociencias PETROBRAS 13,7-25 nov.2004/maio 2005.

944

945 Diniz-Ferreira, E.L. and Torres-Verdín, C., 2012, June. Improved Estimation of Pore
946 Connectivity and Permeability in Deepwater Carbonates with the Construction of Multi-Layer
947 Static and Dynamic Petrophysical Models. In SPWLA 53rd Annual Logging Symposium.
948 Society of Petrophysicists and Well-Log Analysts.

949

950 Doede, A. L., & DeGuzman, P. B. (2020). The disappearing lake: A historical analysis
951 of drought and the Salton Sea in the context of the GeoHealth Framework. GeoHealth, 4(9),
952 e2020GH000271.

953

954 Dorobek, S., Piccoli, L., Coffey, B., Adams, A., 2012. Carbonate rock-forming
955 processes in the Pre-salt "sag" successions of Campos Basin, offshore Brazil: evidence for
956 seasonal, dominantly abiotic carbonate precipitation, substrate controls, and broader geologic
957 implications. In: AAPG Hedberg Conference "Microbial Carbonate Reservoir
958 Characterization", pp. 4-5.

959

960 Demicco, R.V. and Hardie, L.A., 1994. Sedimentary structures and early diagenetic
961 features of shallow marine carbonate deposits. Society of Economic Paleontologists and
962 Mineralogists, Atlas Series 1. Society of Economic Paleontologists, Tulsa.

963

964 Dias-Brito, D., 1992. Ocorrência de calcisferas pelágicas em depósitos carbonáticos do
965 Atlântico Sul: impacto na configuração paleoceanográfica do Tétis cretáceo. Simp. Bacias
966 Cretácicas Brasileiras, 2, pp.30-34.

967

968 Dias-Brito D. 2000. Global stratigraphy, palaeobiogeography and palaeoecology of
969 Albian-Maastrichtian pithonellid calcispheres: impact on Tethys configuration. Cretaceous
970 Research, 21: pp.315-349.

971

972 Doyle, J.A. and JA, D., 1982. Afropollis, a new genus of early angiosperm pollen, with
973 notes on the Cretaceous palynostratigraphy and paleoenvironments of northern Gondwana.

974

975 Duan, H., Ma, R., Xu, X., Kong, F., Zhang, S., Kong, W., Hao, J. and Shang, L., 2009.
976 Two-decade reconstruction of algal blooms in China's Lake Taihu. Environmental Science &
977 Technology, 43(10), pp.3522-3528.

El Desouky, H., Soete, J., Claes, H., Özkul, M., Vanhaecke, F. and Swennen, R., 2015. Novel applications of fluid inclusions and isotope geochemistry in unravelling the genesis of fossil travertine systems. Sedimentology, 62, pp. 27– 56.

Erthal, M.M., Capezzuoli, E., Mancini, A., Claes, H., Soete, J. and Swennen, R., 2017. Shrub morpho-types as indicator for the water flow energy - Tivoli travertine case (Central Italy). Sed. Geol., 347, pp.79–99.

Fabin, C.E., Correia Filho, O.J., Alencar, M.L., Barbosa, J.A., MIRANDA, T.S., Neumann, V.H., Gomes, I.F. and SANTANA, F.R., 2018. Stratigraphic relations of the Ipubi Formation: siliciclastic-evaporitic succession of the Araripe Basin. Anais da Academia Brasileira de Ciências, 90(2), pp.2049-2071.

Fambrini, G.L., da Cunha Silvestre, D., de Menezes-Filho, J.A.B., Da Costa, I.C. and Neumann, V.H.D.M.L., 2019. Architectural and facies characterization of the Aptian fluvial Barbalha Formation, Araripe Basin, NE Brazil. Geological Society, London, Special Publications, 488(1), pp.119-150.

Farias, F., Szatmari, P., Bahniuk, A. and França, A.B., 2019. Evaporitic carbonates in the pre-salt of Santos Basin–Genesis and tectonic implications. Marine and Petroleum Geology, 105, pp.251-272.

Freire, P.T.C., Abagaro, B.T.O., Sousa Filho, F.E., Silva, J.H., Saraiva, A.A.F., Brito, D.D.S. and Viana, B.C., 2013. Pyritization of fossils from the Lagerstätte Araripe Basin, Northeast Brazil, from the Cretaceous period. Pyrite: synthesis, characterization and uses.

Freitas, B. T., Almeida, R. P., Carrera, S. C., Figueiredo, F. T., Turra, B. B., Varejao, F. G., & Assine, M. L., 2017. Aptian sedimentation in the Recôncavo-Tucano-Jatobá Rift System and its tectonic and paleogeographic significance. Journal of South American Earth Sciences, 80, 460-481.

García Ruiz, J.M., 1998. Carbonate precipitation into alkaline silica-rich environments. Geology, 26(9), pp.843-846.

Gindre-Chanu, L., Warren, J.K., Puigdefabregas, C., Sharp, I.R., Peacock, D.C., Swart, R., Poulsen, R., Ferreira, H. and Henrique, L., 2015. Diagenetic evolution of Aptian evaporites in the Namibe Basin (south-west Angola). Sedimentology, 62(1), pp.204-233.

Goebel, N. L., Wing, S. R., & Boyd, P. W., 2005. A mechanism for onset of diatom blooms in a fjord with persistent salinity stratification. Estuarine, Coastal and Shelf Science, 64(2-3), 546-560.

Goldberg, K., Kuchle, J., Scherer, C., Alvarenga, R., Ene, P.L., Armelenti, G. and De Ros, L.F., 2017. Re-sedimented deposits in the rift section of the Campos Basin. Marine and Petroleum Geology, 80, pp.412-431.

Gomes, J. P. B., Bunevich, R.B., Tedeschi, L.R., Tucker, M.E. and Whitaker, F.F., 2020a. Facies classification and patterns of lacustrine carbonate deposition of the Barra Velha Formation, Santos Basin, Brazilian Pre-salt. Marine and Petroleum Geology, 113, p.104176.

Gomes, J. P. B., Bunevich, R. B., Tonietto, S. N., Alves, D. B., Santos, J. F., & Whitaker, F. F. 2020b. Climatic signals in lacustrine deposits of the Upper Yacoraite Formation, Western Argentina: Evidence from clay minerals, analcime, dolomite and fibrous calcite. Sedimentology.

Harris, N.B., 2000. AAPG Memoir 73, Chapter 24: Toca Carbonate, Congo Basin: Response to an Evolving Rift Lake.

Heimhofer, R. and Martill, D., 2007. The sedimentology and depositional environment of the Crato Formation. In: The Crato fossil beds of Brazil: window into an ancient world (pp. 44-63). Cambridge University Press.

Heimhofer, U., Ariztegui, D., Lenniger, M., Hesselbo, S.P., Martill, D.M. and RIOS-NETTO, A.M., 2010. Deciphering the depositional environment of the laminated Crato fossil beds (Early Cretaceous, Araripe Basin, North-eastern Brazil). Sedimentology, 57(2), pp.677-694.

Heine, C., Zoethout, J., Müller, R.D., 2013. Kinematics of the South Atlantic rift. Solid Earth 4, 215–253. https://doi.org/10.5194/se-4-215-2013

1049 Herlinger Jr, R., Zambonato, E.E. and De Ros, L.F., 2017. Influence of diagenesis on
1050 the quality of Lower Cretaceous Pre-salt lacustrine carbonate reservoirs from northern Campos
1051 Basin, offshore Brazil. Journal of Sedimentary Research, 87(12), pp.1285-1313.
1052
1053 Hodelka, B. N., McGlue, M. M., Zimmerman, S., Ali, G., & Tunno, I. (2020).
1054 Paleoproduction and environmental change at Mono Lake (eastern Sierra Nevada) during the
1055 Pleistocene-Holocene transition. Palaeogeography, Palaeoclimatology, Palaeoecology, 543,
1056 109565.
1057
1058 Holmden, C., Creaser, R.A., Muehlenbachs, K.L.S.A., Leslie, S.A. and Bergstrom,
1059 S.M., 1998. Isotopic evidence for geochemical decoupling between ancient epeiric seas and
1060 bordering oceans: implications for secular curves. Geology, 26(6), pp.567-570.
1061
1062 Hosa, A., Wood, R. A., Corbett, P. W. M., de Souza, R. S., & Roemers, E., 2020.
1063 Modelling the impact of depositional and diagenetic processes on reservoir properties of the
1064 crystal-shrub limestones in the 'Pre-Salt'Barra Velha Formation, Santos Basin, Brazil. Marine
1065 and Petroleum Geology, 112, 104100.
1066
1067 Immenhauser, A., Della Porta, G., Kenter, J.A. and Bahamonde, J.R., 2003. An
1068 alternative model for positive shifts in shallow-marine carbonate $\delta^{13}C$ and
1069 $\delta^{18}O$. Sedimentology, 50(5), pp.953-959.
1070
1071 Jones, B.F., 1986. Clay mineral diagenesis in lacustrine sediments. In: Studies in
1072 Diagenesis. Ed. Mumpton, F.A. United States Geological Survey Bulletin, 1578, pp.291-300.
1073

Kiage, L. M., & Douglas, P. (2020). Linkages between land cover change, lake shrinkage, and sublacustrine influence determined from remote sensing of select Rift Valley Lakes in Kenya. Science of The Total Environment, 709, 136022.

Kirkham, A. and Tucker, M.E., 2018. Thrombolites, spherulites and fibrous crusts (Holkerian, Purbeckian, Aptian): Context, fabrics and origins. Sedimentary geology, 374, pp.69-84.

Lima, B.E.M. and De Ros, L.F., 2019. Deposition, diagenetic and hydrothermal processes in the Aptian Pre-Salt lacustrine carbonate reservoirs of the northern Campos Basin, offshore Brazil. Sedimentary geology, 383, pp.55-81.

Lagaly, G., Schulz, O. and Zimehl, R. 1997. Dispersionen und Emulsionen: eine Einführung in die Kolloidik feinverteilter Stoffe einschließlich der Tonminerale. Steinkopff, Darmstadt.

Larsen, C.P.S., Pienitz, R., Smol, J.P., Moser, K.A., Cumming, B.F., Blais, J.M., Macdonald, G.M. and Hall, R.I., 1998. Relations between lake morphometry and the presence of laminated lake sediments: a re-examination of Larsen and MacDonald (1993). Quaternary Science Reviews, 17(8), pp.711-717.

Lepley, S., Piccoli, L., Chitale, V., Kelley, I. and Quest, M., 2017. The Importance of Understanding Diagenesis for the Development of Pre-Salt Lacustrine Carbonates. In AAPG Annual Convention and Exhibition.

Lima, B.E.M., Tedeschi, L.R., Pestilho, A.L.S., Santos, R.V., Vazquez, J.C., Guzzo, J.V.P. and De Ros, L.F., 2020. Deep-burial hydrothermal alteration of the Pre-Salt carbonate reservoirs from northern Campos Basin, offshore Brazil: Evidence from petrography, fluid inclusions, Sr, C and O isotopes. Marine and Petroleum Geology, 113, p.104143.

de Luca, P.H.V., Matias, H., Carballo, J., Sineva, D., Pimentel, G.A., Tritlla, J., Esteban, M., Loma, R., Alonso, J.L.A., Jiménez, R.P. and Pontet, M., 2017. Breaking barriers and paradigms in presalt exploration: the Pão de Açúcar discovery (offshore Brazil).

Maisey, J.G., 1990. Stratigraphy and depositional environment of the Crato member (Santana Formation, Lower Cretaceous of NE Brazil). Insects from the Santana Formation, Lower Cretaceous, of Brazil. Bulletin of the American Museum of Natural History, 195(191), pp.15-19.

Maisey, J.G., 1996. Non-marine occurrence of ichthyodectiforms in the Lower Cretaceous of Brazil. Journal of Vertebrate Paleontology, 16(3).

Mancini, A., Capezzuoli, E., Erthal M., Swennen, R., 2018, Hierarchical approach to define travertine depositional systems: 3D conceptual morphological model and possible applications. Marine and Petroleum geology, 103, pp. 549-563.

Mariotti, G., Pruss, S.B., Perron, J.T. and Bosak, T., 2014. Microbial shaping of sedimentary wrinkle structures. Nature Geoscience, 7(10), pp.736-740.

Martill, D.M., FREY, E. and LOVERIDGE, R., 2006. The taphonomy of the allochthonous palaeobiota of the Crato Formation (Lower Cretaceous) of Brazil. Mesozoic Terrestrial Ecosystems, 2006, pp.71-75.

Martill, D.M. and Wilby, P.R., 1993. Stratigraphy. 20–50. Fossils of the Santana and Crato formations, Brazil. Palaeontological Association, London, Field Guides to Fossils, 5, p.158.

Martill, D.M., Bechly, G. and Loveridge, R.F., 2007. The Crato fossil beds of Brazil: window into an ancient world. Cambridge University Press.

Martill, D.M., Loveridge, R.F. and Heimhofer, U., 2008. Dolomite pipes in the Crato Formation fossil lagerstätte (Lower Cretaceous, Aptian), of northeastern Brazil. Cretaceous Research, 29(1), pp.78-86.

Martill, D.M., 1993. Fossils of the Santana and Crato Formations, Brazil. Palaeontological Association.

McCormack, J., Nehrke, G., Jöns, N., Immenhauser, A. and Kwiecien, O., 2019. Refining the interpretation of lacustrine carbonate isotope records: Implications of a mineralogy-specific Lake Van case study. Chemical Geology, 513, pp.167-183.

Meinhold, G., Jensen, S., Høyberget, M., Arslan, A., Ebbestad, J.O.R., Högström, A.E., Palacios, T., Agić, H. and Taylor, W.L., 2019. First record of carbonates with spherulites and

1146 cone-in-cone structures from the Precambrian of Arctic Norway, and their
1147 palaeoenvironmental significance. Precambrian Research, 328, pp.99-110.
1148
1149 Meister, P., Johnson, O., Corsetti, F., & Nealson, K. H., 2011. Magnesium inhibition
1150 controls spherical carbonate precipitation in ultrabasic springwater (Cedars, California) and
1151 culture experiments. In Advances in Stromatolite Geobiology (pp. 101-121). Springer, Berlin,
1152 Heidelberg.
1153 Mello, M.R., Koutsoukos, E.A., Mohriak, W.U. and Bacoccoli, G., 1994. Selected
1154 Petroleum Systems in Brazil: Chapter 31: Part V. Case Studies--Western Hemisphere. In:
1155 Magoon, L.B. and Dow W.G. (Eds.) The Petroleum system – from source to trap. AAPG
1156 Memoirs, 60, pp. 499-512.
1157
1158 Mello, M.R., 2006. 3D petroleum system modeling and exploration risk assessment of
1159 the greater Campos Basin: go deep for giant oil and gas field. In: Rio Oil and Gas Expo and
1160 Conference, 1. Anais, Rio de Janeiro.
1161
1162 Mendoza, M. E., Bocco, G., Bravo, M., Granados, E. L., & Osterkamp, W. R. (2006).
1163 Predicting water-surface fluctuation of continental lakes: a RS and GIS based approach in
1164 Central Mexico. Water Resources Management, 20(2), 291-311.
1165
1166 Menon, F., and Martill, D., 2007. Taphonomy and preservation of Crato Formation
1167 arthropods. In The Crato fossil beds of Brazil: Window into an ancient world (pp. 79-96).
1168 Cambridge University Press.
1169 Mercedes-Martín, R., Rogerson, M.R., Brasier, A.T., Vonhof, H.B., Prior, T.J.,
1170 Fellows, S.M., Reijmer, J.J.G., Billing, I. and Pedley, H.M., 2016. Growing spherulitic calcite

grains in saline, hyperalkaline lakes: experimental evaluation of the effects of Mg-clays and organic acids. Sedimentary geology, 335, pp.93-102.

Mercedes-Martín, R., Brasier, A.T., Rogerson, M., Reijmer, J.J., Vonhof, H. and Pedley, M., 2017. A depositional model for spherulitic carbonates associated with alkaline, volcanic lakes. Marine and petroleum geology, 86, pp.168-191.

Mercedes-Martín, R., Ayora, C., Tritlla, J. and Sánchez-Román, M., 2019. The hydrochemical evolution of alkaline volcanic lakes: a model to understand the South Atlantic Pre-salt mineral assemblages. Earth-Science Reviews, p.102938.

Mercedes-Martín, R., Rao, A., Rogerson, M., & Sánchez-Román, M., 2020. Effects of Salinity, Organic Acids and Alkalinity in the Growth of Calcite Spherulites: Implications for Evaporitic Lacustrine Sedimentation. The Depositional Record. DOI: 10.1002/dep2.136.

Miranda, T.S., Santos, R.F., Barbosa, J.A., Gomes, I.F., Alencar, M.L., Correia, O.J., Falcão, T.C., Gale, J.F.W. and Neumann, V.H., 2018. Quantifying aperture, spacing and fracture intensity in a carbonate reservoir analogue: Crato Formation, NE Brazil. Marine and Petroleum Geology, 97, pp.556-567.

Mohammadi, Z., Capezzuoli, E., Claes, H., Alipoor, R., Muchez, P. and Swennen, R., 2019. Substrate geology controlling different morphology, sedimentology, diagenesis and geochemistry of adjacent travertine bodies: a case study from the Sanandaj-Sirjan zone (western Iran). Sedimentary Geology, 389, 127–146.

Mohammadi, Z., Claes, H., Capezzuoli, E., Mozafari, M., Soete, J., Aratman, C. and Swennen, R., 2020a. Lateral and vertical variations in sedimentology and geochemistry of sub-horizontal laminated travertines (Çakmak quarry, Denizli Basin, Turkey), Quat. Int. 540, pp. 146-168. https://doi.org/10.1016/j.quaint.2018.11.041.

Mohammadi, Z., Vaselli, O., Muchez, P. Bouillon, S., Claes, H., Capezzuoli, E., and Swennen, R., 2020b. Hydrogeochemistry, stable isotope composition and geothermometry of CO2-bearing hydrothermal springs from Western Iran: Evidence for their origin, evolution and spatio-temporal variations. Sedimentary Geology, 404, 105676.

Monaghan, P.H. and Lytle, M.L., 1956. The origin of calcareous ooliths. Journal of Sedimentary Research, 26(2), pp.111-118.

Moore, D. M. and Reynolds, R. C. 1997. X-Ray Diffraction and the Identification and Analyses of Clay Minerals. second edition. Oxford University Press, New York.

Muniz, M.C. and Bosence, D.W.J., 2015. Pre-salt microbialites from the Campos Basin (offshore Brazil): image log facies, facies model and cyclicity in lacustrine carbonates. Geological Society, London, Special Publications, 418(1), pp.221-242.

Neumann, V.H., Borrego, A.G., Cabrera, L. and Dino, R., 2003. Organic matter composition and distribution through the Aptian–Albian lacustrine sequences of the Araripe Basin, northeastern Brazil. International Journal of Coal Geology, 54(1-2), pp.21-40.

Neumann, V.H., 1999. Estratigrafía, Sedimentología, Geoquímica y Diagénesis de los sistemas lacustres Aptiense–Albienses de la Cuenca de Araripe (NE Brasil). PhD Thesis. Barcelona University. 233 pp.

Nakano, C.M.F., Pinto, A.C.C., Marcusso, J.L., Minami, K., 2009. Pre-salt Santos Basin-Extended well test and Production Pilot in the Tupi area-the Planning phase. In: Offshore Technology Conference, pp. 1-8.

Nof, R. N., Ziv, A., Doin, M. P., Baer, G., Fialko, Y., Wdowinski, S., ... & Bock, Y. (2012). Rising of the lowest place on Earth due to Dead Sea water-level drop: Evidence from SAR interferometry and GPS. Journal of Geophysical Research: Solid Earth, 117(B5).

Null, S. E., & Wurtsbaugh, W. A. (2020). Water development, consumptive water uses, and Great Salt Lake. In Great Salt Lake Biology (pp. 1-21). Springer, Cham.

O'sullivan, P.E., 1983. Annually-laminated lake sediments and the study of Quaternary environmental changes—a review. Quaternary Science Reviews, 1(4), pp.245-313.

Ojala, A.E., Saarinen, T. and Salonen, V.P., 2000. Preconditions for the formation of annually laminated lake sediments in southern and central Finland. Boreal Environment Research, 5(3), pp.243-255.

Oppenheimer, C.H., 1961. Note on the formation of spherical aragonitic bodies in the presence of bacteria from the Bahama Bank. Geochimica et Cosmochimica Acta, 23, pp.295-296.

Pentecost, A., 2005. Travertine. Springer Science & Business Media.

Pérez, E., & Chebude, Y. (2017). Chemical analysis of Gaet'ale, a hypersaline pond in Danakil Depression (Ethiopia): New record for the most saline water body on Earth. Aquatic Geochemistry, 23(2), 109-117.

Pietzsch, R., Oliveira, D. M., Tedeschi, L. R., Neto, J. V. Q., Figueiredo, M. F., Vazquez, J. C., & de Souza, R. S. (2018). Palaeohydrology of the Lower Cretaceous pre-salt lacustrine system, from rift to post-rift phase, Santos Basin, Brazil. Palaeogeography, Palaeoclimatology, Palaeoecology, 507, 60-80.

Pietzsch, R., Tedeschi, L.R., Oliveira, D.M., dos Anjos, C.W.D., Vazquez, J.C. and Figueiredo, M.F., 2020. Environmental conditions of deposition of the Lower Cretaceous lacustrine carbonates of the Barra Velha Formation, Santos Basin (Brazil), based on stable carbon and oxygen isotopes: A continental record of pCO2 during the onset of the Oceanic Anoxic Event 1a (OAE 1a) interval?. Chemical Geology, p.119457.

Pons, D., Berthou, P.Y. and De Almeida Campos, D., 1990, June. Quelques observations sur la palynologie de l'Aptien Supérieur et de l'Albien du Bassin d'Araripe (NE du Brésil). In Simposio sobre a Bacia do Araripe e bacias interiores do Nordeste, pp. 241-252.

Ray, D. C., van Buchem, F. S., Baines, G., Davies, A., Gréselle, B., Simmons, M. D., & Robson, C., 2019. The magnitude and cause of short-term eustatic Cretaceous sea-level change: A synthesis. Earth-Science Reviews, 197, 102901.

Regnet, J.B., Fortin, J., Nicolas, A., Pellerin, M. and Guéguen, Y., 2018. Elastic properties of continental carbonates: From controlling factors to an applicable model for acoustic-velocity predictions. Geophysics, 84(1), pp.MR45-MR59.

Renaut, R. W., Owen, R. B., & Ego, J. K. (2017). Geothermal activity and hydrothermal mineral deposits at southern Lake Bogoria, Kenya Rift Valley: Impact of lake level changes. Journal of African Earth Sciences, 129, 623-646.

Rezende, M.F., Pope, M.C., 2015. Importance of depositional texture in pore characterization of subsalt microbialite carbonates, offshore Brazil. Geol. Soc. Lond. Spec. Publ. 418.

Riding, R. (2000). Microbial carbonates: the geological record of calcified bacterial–algal mats and biofilms. Sedimentology, 47, 179-214.

Riding, R., & Virgone, A., 2020. Hybrid Carbonates: in situ abiotic, microbial and skeletal co-precipitates. Earth-Science Reviews, 103300.

Rodrigues, M. G., Matos, S. A., Varejão, F. G., Fürsich, F. T., Warren, L. V., Assine, M. L., and Simões, M. G., 2020. Short-lived “bakevelliid-sea” in the Aptian Romualdo Formation, Araripe Basin, northeastern Brazil. Cretaceous Research, 104555.

Rogerson, M., Mercedes-Martín, R., Brasier, A.T., McGill, R.A., Prior, T.J., Vonhof, H., Fellows, S.M., Reijmer, J.J., McClymont, E., Billing, I. and Matthews, A., 2017. Are spherulitic lacustrine carbonates an expression of large-scale mineral carbonation? A case study from the East Kirkton Limestone, Scotland. Gondwana Research, 48, pp.101-109.

Ronchi, P. and Cruciani, F., 2015. Continental carbonates as a hydrocarbon reservoir, an analog case study from the travertine of Saturnia, Italy. AAPG Bulletin, 99(4), pp.711-734.

Reeves Jr, C.C., 1968. Introduction to Paleolimnology. Developments in Sedimentology, 11, Chapter 5: Lacustrine Sediments: Chemical Precipitates and Chapter 6: Lacustrine Sediments: Clastic.

Reid, R.P., Visscher, P.T., Decho, A.W., Stolz, J.F., Bebout, B.M., Dupraz, C., Macintyre, I.G., Paerl, H.W., Pinckney, J.L., Prufert-Bebout, L. and Steppe, T.F., 2000. The role of microbes in accretion, lamination and early lithification of modern marine stromatolites. Nature, 406(6799), pp.989-992.

Saarnisto, 1986. Annually laminated lake sediments in B.E. Berglund (Ed.), Handbook of Holocene Palaeoecology and Palaeohydrology, John Wiley and Sons, Chichester (1986), pp. 343-370

Saller, A., Rushton, S., Buambua, L., Inman, K., Mcneil, R., Dickson, J.A.D.T., 2016. Presalt stratigraphy and depositional systems in the Kwanza Basin, offshore Angola. AAPG Bull. 100 (7), 1135e1164.

Sánchez-Navas, A., Martín-Algarra, A., Rivadeneyra, M.A., Melchor, S. and Martín-Ramos, J.D., 2009. Crystal-growth behavior in Ca− Mg carbonate bacterial spherulites. Crystal Growth and Design, 9(6), pp.2690-2699.

Scherer, C. M., Goldberg, K. and Bardola, T., 2015. Facies architecture and sequence stratigraphy of an early post-rift fluvial succession, Aptian Barbalha Formation, Araripe Basin, northeastern Brazil. Sedimentary Geology, 322, pp. 43-62.

Schulz, S., Darehshouri, S., Hassanzadeh, E., Tajrishy, M., & Schüth, C. (2020). Climate change or irrigated agriculture–what drives the water level decline of Lake Urmia. Scientific reports, 10(1), 1-10.

Schoellkopf, N.B. and Patterson, B.A., 2000. Petroleum systems of Cabinda, Angola. Petroleum Systems of South Atlantic Margins. American Association of Petroleum Geologists Memoirs, 73, pp.361-376.

Schröder, S., Ibekwe, A., Saunders, M., Dixon, R., Fisher, A., 2015. Algal-microbial carbonates of the Namibe Basin (Albian, Angola): implications for microbial carbonate mound development in the South Atlantic. Pet. Geosci. 2014-2083.

Seard, C., Camoin, G., Rouchy, J.M. and Virgone, A., 2013. Composition, structure and evolution of a lacustrine carbonate margin dominated by microbialites: Case study from the Green River Formation (Eocene; Wyoming, USA). Palaeogeography, Palaeoclimatology, Palaeoecology, 381, pp.128-144.

Self, C.A. and Hill, C.A., 2003. How speleothems grow: an introduction to the ontogeny of cave minerals. Journal of Cave and Karst Studies, 65(2), pp.130-151.

Senner, N. R., Moore, J. N., Seager, S. T., Dougill, S., Kreuz, K., & Senner, S. E. (2018). A salt lake under stress: Relationships among birds, water levels, and invertebrates at a Great Basin saline lake. Biological Conservation, 220, 320-329.

Shtukenberg, A. G., Punin, Y. O., Gunn, E., & Kahr, B., 2012. Spherulites. Chemical reviews, 112(3), 1805-1838.

Silva-Telles, J., Augusto, A., Mitsuru, H. and Gilberto, I., 1994. Evidences of the first marine ingressions during the East Brazilian margin rift phase; Evidencias das primeiras ingressoes marinhas na fase rift da margem leste brasileira. Boletim de Gociencias da Petrobras, 8, 409-410.

Soete, J., Kleipool, L.M., Claes, H., Claes, S., Hamaekers, H., Kele, S., Özkul, M., Foubert, A., Reijmer, J.J.G., Swennen, R., 2015. Acoustic properties in travertines and their relation to porosity and pore types. Mar. Petrol. Geol. 59, pp.320-335. http://dx.doi.org/10.1016/j.marpetgeo.2014.09.004.

Soete, J., Claes, S., Claes, H., Janssens, N., Cnudde, V., Huysmans, M. and Swennen, R. (2017) Lattice Boltzmann simulations of fluid flow in continental carbonate reservoir rocks and in upscaled rock models generated with multiple-point geostatistics. Geofluids, Special issue: Flow and Transport in Porous Media: A Multiscale Focus. 24 pp.

Souza, R.S., Arienti, L.M., Viana, S.M., Falcão, L.C., Cuglieri, M.A., Silva Filho, R.P., Leite, C.O., Oliveira, V.C., Oliveira, D.M., Anjos, C. and Amora, R., 2018. Petrology of the Hydrothermal and Evaporitic Continental Cretaceous (Aptian) Pre-Salt Carbonates and Associated Rocks, South Atlantic Santos Basin, Offshore Brazil. In AAPG ACE 2018.

Spadafora, A., Perri, E., McKenzie, J.A. and Vasconcelos, C., 2010. Microbial biomineralization processes forming modern Ca: Mg carbonate stromatolites. Sedimentology, 57(1), pp.27-40.

Sun, C.Y., Marcus, M.A., Frazier, M.J., Giuffre, A.J., Mass, T. and Gilbert, P.U., 2017. Spherulitic growth of coral skeletons and synthetic aragonite: nature's three-dimensional printing. ACS nano, 11(7), pp.6612-6622.

Taylor, G.H., Teichmüller, M., Davis, A.C.F.K., Diessel, C.F.K., Littke, R. and Robert, P., 1998. Organic petrology.

Teboul, P.A., Durlet, C., Gaucher, E.C., Virgone, A., Girard, J.P., Curie, J., Lopez, B., Camoin, G.F., 2016. Origins of elements building travertine and tufa: new perspectives provided by isotopic and geochemical tracers. Sediment. Geol. 334, pp. 97–114.

Teboul, P.A., Kluska, J.M., Marty, N.C., Debure, M., Durlet, C., Virgone, A. and Gaucher, E.C., 2017. Volcanic rock alterations of the Kwanza Basin, offshore Angola-Insights from an integrated petrological, geochemical and numerical approach. Marine and Petroleum Geology, 80, pp.394-411.

Teboul, P.A., Durlet, C., Girard, J.P., Dubois, L., San Miguel, G., Virgone, A., Gaucher, E.C. and Camoin, G., 2019. Diversity and origin of quartz cements in continental carbonates: Example from the Lower Cretaceous rift deposits of the South Atlantic margin. Applied geochemistry, 100, pp.22-41.

Terra, G.J.S., et al., 2010. Carbonate rock classification applied to Brazilian sedimentary basins. Bol. Geociencias Petrobras 18 (1), pp. 9-29.

Thompson, L. and Oftebro, C., 2011. Salt gets in your eyes geological challenges and solutions to sub-salt exploration. First Break 29, 93-98. March.

Thompson, D.L., Stilwell, J.D. and Hall, M., 2015. Lacustrine carbonate reservoirs from Early Cretaceous rift lakes of Western Gondwana: Pre-salt coquinas of Brazil and West Africa. Gondwana Research, 28(1), pp.26-51.

Török, Á., Claes, H., Brogi, A., Liotta, D., Tóth, Á., Mindszenty, A., Kudó, I., Kele, S., Huntington, K.W., Shen, C.C. and Swennen, R. (2019) A multi–methodological approach to reconstruct the configuration of a travertine fissure ridge system: The case of the Cukor quarry (Süttő, Gerecse Hills, Hungary). Geomorphology, 106836. doi.org/10.1016/j.geomorph.2019.106836.

Török, Á (2018) The anatomy of a Pleistocene travertine complex. Sedimentological, diagenetic and reservoir studies on the Süttö travertine system (Gerecse Hills, Hungary).

Dissertation in partial fulfilment of the requirements for the degree of Doctor of Science (PhD): Geology. KU Leuven – ELTE.

Tutolo, B.M. and Tosca, N.J., 2018. Experimental examination of the Mg-silicate-carbonate system at ambient temperature: Implications for alkaline chemical sedimentation and lacustrine carbonate formation. Geochimica et Cosmochimica Acta, 225, pp.80-101.

Tosca, N.J. and Wright, V.P., 2018. Diagenetic pathways linked to labile Mg-clays in lacustrine carbonate reservoirs: a model for the origin of secondary porosity in the Cretaceous pre-salt Barra Velha Formation, offshore Brazil. Geological Society, London, Special Publications, 435(1), pp.33-46.

Tracy, S.L., François, C.J.P. and Jennings, H.M., 1998a. The growth of calcite spherulites from solution: I. Experimental design techniques. Journal of crystal growth, 193(3), pp.374-381.

Tracy, S.L., Williams, D.A. and Jennings, H.M., 1998b. The growth of calcite spherulites from solution: II. Kinetics of formation. Journal of Crystal Growth, 193(3), pp.382-388.

Turner, E.C. and Jones, B., 2005. Microscopic calcite dendrites in cold-water tufa: Implications for nucleation of micrite and cement. Sedimentology, 52(5), pp.1043-1066.

Tweed, S., Leblanc, M., & Cartwright, I. (2009). Groundwater–surface water interaction and the impact of a multi-year drought on lakes conditions in South-East Australia. Journal of Hydrology, 379(1-2), 41-53.

Tylmann, W., Szpakowska, K., Ohlendorf, C., Woszczyk, M. and Zolitschka, B., 2012. Conditions for deposition of annually laminated sediments in small meromictic lakes: a case study of Lake Suminko (northern Poland). Journal of Paleolimnology, 47(1), pp.55-70.

Tyson, 1984, 1993, 1995;

Ufer, K., Kleeberg, R., Bergmann, J., Curtius, H. and Dohrmann, R., 2008. Refining real structure parameters of disordered layer structures within the Rietveld method. Zeitschrift für Kristallographie Supplements, 27, pp.151-158.

Valente da Silva, B., Pereira, G.D.C.R., Oliveira, E.C. and Bergamaschi, S., 2017. Petrographic Study of Silica-rich Continental Carbonates from São José de Itaboraí Basin (Brazil). Journal of Sedimentary Environments, 2(4), pp.319-328.

Van Noten, K., Claes, H., Soete, J., Foubert, A., Özkul, M. and Swennen, R., 2013. Fracture networks and strike-slip deformation along reactivated normal faults in Quaternary travertine deposits, Denizli Basin, Western Turkey. Tectonophysics, 588, pp. 154–170.

Van Noten, K., Topal, S., Baykara, M.O., Özkul, M., Claes, H., Aratman, C. and Swennen, R., 2019. Pleistocene-Holocene tectonic reconstruction of the Ballik travertine (Denizli Graben, SW Turkey): (de)formation of large travertine geobodies at intersecting grabens. J. Struct. Geol., 118, pp. 114–134.

Virgone, A., Broucke, O., Held, A.E., Lopez, B., Seard, C., Camoin, G., Swennen, R., Foubert, A., Rouchy, J.M., Pabian-Goyheneche, C. and Guo, L., 2013, March. Continental carbonates reservoirs: the importance of analogues to understand presalt discoveries. In IPTC 2013: International Petroleum Technology Conference.

Varejao, F.G., Warren, L.V., de Jesus Perinotto, J.A., Neumann, V.H., Freitas, B.T., de Almeida, R.P. and Assine, M.L., 2016. Upper Aptian mixed carbonate-siliciclastic sequences from Tucano Basin, Northeastern Brazil: implications for paleogeographic reconstructions following Gondwana break-up. Cretaceous Research, 67, pp.44-58.

Varejão, F.G., Warren, L.V., Freitas, B.T., Neumann, V.H. and Assine, M.L., 2019. Saline lake development in the Aptian post-rift phase of the Tucano Basin: Tectonic and paleogeographic implications. Journal of South American Earth Sciences, 92, pp.282-297.

Vasconcelos, C., Dittrich, M. and McKenzie, J.A., 2014. Evidence of microbiocoenosis in the formation of laminae in modern stromatolites. Facies, 60(1), pp.3-13.

Verrecchia, E.P., Freytet, P., Verrecchia, K.E. and Dumont, J.L., 1995. Spherulites in calcrete laminar crusts; biogenic CaCO 3 precipitation as a major contributor to crust formation. Journal of Sedimentary research, 65(4a), pp.690-700.

Wanas, H.A., 2012. Pseudospherulitic fibrous calcite from the Quaternary shallow lacustrine carbonates of the Farafra Oasis, Western Desert, Egypt: a primary precipitate with possible bacterial influence. Journal of African Earth Sciences, 65, pp.105-114.

Warren, L.V., Varejão, F.G., Quaglio, F., Simões, M.G., Fürsich, F.T., Poiré, D.G., Catto, B. and Assine, M.L., 2017. Stromatolites from the Aptian Crato Formation, a hypersaline lake system in the Araripe Basin, northeastern Brazil. Facies, 63(1), p.3.

Wasson, M.S., Saller, A., Andres, M., Self, D. and Lomando, A., 2012, June. Lacustrine microbial carbonate facies in core from the lower Cretaceous Toca Formation, Block 0, offshore Angola. In Am. Assoc. Pet. Geol. Hedberg Conf.'Microbial Carbonate Reserv. Charact. Houst. TX (pp. 4-8).

Williams, W. D. (1995). Lake Corangamite, Australia, a permanent saline lake: conservation and management issues. Lakes & Reservoirs: Research & Management, 1(1), 55-64.

Wright, P. and Barnett, A., 2014. Cyclicity and carbonate-silicate gel interactions in Cretaceous alkaline lakes. AAPG Search and Discovery Article, 51011, pp.6-9.

Wright, V.P. and Barnett, A.J., 2015. An abiotic model for the development of textures in some South Atlantic early Cretaceous lacustrine carbonates. Geological Society, London, Special Publications, 418(1), pp.209-219.

Wright, V.P. and Barnett, A.J., 2020. The textural evolution and ghost matrices of the Cretaceous Barra Velha Formation carbonates from the Santos Basin, offshore Brazil. Facies, 66(1), p.7.

Wright, P. and Rodriguez, K., 2018. Reinterpreting the South Atlantic pre-salt 'microbialite'reservoirs: Petrographic, isotopic and seismic evidence for a shallow evaporitic lake depositional model. First Break, 36(5), pp.71-77.

Wright, V.P., 2012. Lacustrine carbonates in rift settings: the interaction of volcanic and microbial processes on carbonate deposition. Geol. Soc. Lond. Spec. Publ. 370 (1), 39e47. http://dx.doi.org/10.1144/SP370.2.

Wright, P. and Tosca, N., 2016. A geochemical model for the formation of the pre-salt reservoirs, Santos Basin, Brazil: Implications for understanding reservoir distribution. AAPG Search and Discovery, Article, 51304.

Wu, S., Blake, J. I., Guo, L., & Zhou, W., 2020. Naturally Occurring and Biomimetic Synthesized Calcite Spherulites. Crystal Growth & Design, 20(5), 3537-3545.

Zhou, J., Wu, J., Long, M., & Qiang, M. (2019). Late Quaternary lake-level and climate changes in arid central Asia inferred from sediments of Ebinur Lake, Xinjiang, northwestern China. Quaternary Research, 92(2), 416-429.

Ziegler, A., Eshel, G., Rees, P.M., Rothfus, T., Rowley, D. and Sunderlin, D., 2003. Tracing the tropics across land and sea: Permian to present. Lethaia, 36(3), pp.227-254.

Zola, R. P., & Bengtsson, L. (2006). Long-term and extreme water level variations of the shallow Lake Poopó, Bolivia. Hydrological Sciences Journal, 51(1), 98-114.

1540

1541